Insights into bacterial lipoprotein trafficking from a structure of LolA bound to the LolC periplasmic domain

Elise Kaplan, Nicholas P. Greene, Allister Crow [‡], *Vassilis Koronakis* *

Department of Pathology, University of Cambridge, UK.

[‡] Current address: School of Life Sciences, University of Warwick, UK.

***Corresponding author: vk103@cam.ac.uk**

Running title: Structure of LolA bound to the LolC periplasmic domain

Abstract

In Gram-negative bacteria, outer membrane lipoproteins are essential for maintaining cellular integrity, transporting nutrients, establishing infections and promoting the formation of biofilms. The LolCDE ABC transporter, LolA chaperone, and LolB outer membrane receptor form an essential system for transporting newly-matured lipoproteins from the outer leaflet of the cytoplasmic membrane to the innermost leaflet of the outer membrane. Here, we present a crystal structure of LolA in complex with the periplasmic domain of LolC. The structure reveals how a solvent-exposed β-hairpin loop (termed the 'Hook') and trio of surface residues (the 'Pad') of LolC are essential for recruiting LolA from the periplasm and priming it to receive lipoproteins. Experiments with purified LolCDE complex demonstrate that association with LolA is independent of nucleotide binding and hydrolysis, and homology models based on the MacB ABC transporter predict that LolA recruitment takes place at a periplasmic site located at least 50 Å from the inner membrane. Implications for the mechanism of lipoprotein extraction and transfer are discussed. The LolA·LolC structure provides atomic details on a key protein interaction within the Lol pathway and constitutes a vital step toward the complete molecular understanding of this important system.

Significance

The outer membrane of Gram-negative bacteria presents a selectively-permeable barrier to the environment and is the first line of defence against antibiotics and other antimicrobial agents. Maintenance of the outer membrane relies on lipoproteins delivered by the LolABCDE system making the Lol proteins attractive targets for the development of new antimicrobial compounds. During trafficking, lipoproteins are extracted from the cytoplasmic membrane by the LolCDE complex, transported across the periplasm by LolA and integrated into the outer membrane by LolB. Here, we describe structural features underpinning the interaction between LolA and LolCDE. The structure of

LolA bound to the periplasmic domain of LolC provides an arresting molecular snapshot of a key intermediate in the bacterial lipoprotein trafficking pathway.

Keywords

Lipoprotein trafficking, Protein interactions, Membrane biogenesis, X-ray crystallography, ABC transporter.

Introduction

In Gram-negative bacteria, the outer membrane provides an important physical barrier to the extracellular space protecting against osmotic shock, noxious compounds and antibiotics (1, 2). Lipoproteins, anchored by N-terminally linked acyl groups, are a crucial structural component of the outer membrane maintaining attachment to the peptidoglycan layer (3, 4). Other lipoproteins underpin assembly of integral β-barrel proteins at the outer membrane (1, 5, 6), insertion of lipopolysaccharide (7, 8), maintenance of outer membrane lipid asymmetry (9, 10) and regulation of peptidoglycan synthesis (11). Lipoproteins are therefore central to the physiology of the cell envelope. Mislocalisation of outer membrane lipoproteins on the inner membrane results in cell death (12, 13) and proteins responsible for lipoylation and trafficking of outer membrane lipoproteins are essential for bacterial viability (14–18). The relative accessibility of proteins involved in lipoprotein maturation and trafficking, combined with their essential functions, have made these systems attractive targets for developing new antimicrobial agents (19–21).

Maturation of bacterial lipoproteins is a multistep process (**Fig. 1**). Lipoproteins are first produced in 'prepro' form in the cytoplasm and require transport across the inner membrane by the Sec pathway (22). Once integrated into the membrane, preprolipoproteins are subject to a series of modifications by enzymes recognising a cluster of four sequential amino acids termed the lipobox (22). Addition of the fatty acyl groups is accomplished by the sequential action of three enzymes: Lgt, Lsp and Lnt. Firstly, Lgt catalyses addition of diacylglycerol to the lipobox cysteine residue before Lsp removes the N-terminal transmembrane anchor. Finally, Lnt acetylates the N-terminal amino group of the cysteine resulting in the mature, triacylated, form (22). Lipoproteins bearing an aspartate at position 2 of the lipobox are retained in the inner membrane (23), and mature lipoproteins destined for the outer membrane are transported by the Lol system, which, in *E. coli,* is composed of five proteins, LolABCDE (14, 15, 24).

The LolCDE complex is an ABC transporter that comprises a heterodimer of the transmembrane proteins LolC and LolE, and a homodimer of cytoplasmic LolD, which forms the nucleotide binding domain (NBD) that hydrolyses ATP. LolCDE is responsible for the energetically costly extraction of

lipoproteins from the inner membrane and their transfer to LolA, a periplasmic chaperone. Lipoproteins bound to LolA are transported across the periplasm and accepted by the outer membrane receptor LolB, itself a lipoprotein, which mediates substrate integration into the outer membrane (14, 16). Though *E. coli* LolA and LolB have similar β-barrel folds (25), they perform distinct roles (26).

Transfer of lipoproteins between LolA and LolB is proposed to proceed by 'mouth-to-mouth' exchange between the central barrels of these proteins (27). NMR and *in vivo* crosslinking experiments support the mouth-to-mouth model through identification of contacting residues in LolA and LolB that map to the rim of the barrel during complex formation (27, 28). *In vivo* crosslinking studies have also demonstrated that in *E. coli*, LolC and LolE have distinct roles. LolC interacts with the LolA chaperone while LolE binds lipoproteins, but the molecular details of these interactions are not clear (27, 29). In other organisms, including pathogens such as *Francisella tularensis* and *Acinetobacter baumannii*, such division of labour does not exist and LolF replaces both LolC and LolE in a symmetric, LolDF assembly (30).

The LolCDE complex belongs to the ABC3 superfamily of ABC transporters, which includes the tripartite efflux pump component MacB and the FtsEX cell division machinery (31, 32). Unlike canonical ABC transporters, ABC3 members (also known as Type VII ABC transporters) (33) are not proposed to transport substrates across the membrane in which they are embedded. At present, MacB, a toxin and antibiotic transporter (33–35), is the only representative of the ABC3 family to be structurally characterised (33, 36–38). Each monomer of the MacB homodimer has a distinctive 4-transmembrane helix topology and an N-terminally fused NBD. A large periplasmic domain, composed of so-called Porter and Sabre subdomains is elevated ~25 Å above the membrane by a helical stalk composed of extensions of the first and second transmembrane helices (TM1 and TM2). A shorter periplamic loop, termed the Shoulder, links TM3 and TM4. Comparison of ATP-bound (33) and nucleotide-free (37) structures indicates that MacB undergoes impressive conformational changes, termed 'mechanotransmission', during its ATP binding and hydrolysis cycle. Mechanotransmission couples cytoplasmic ATP hydrolysis with periplasmic conformational changes used to perform work in the periplasm/extracytoplasmic space (33). LolC and LolE have the same transmembrane topology as MacB (39), and the periplasmic domain has the same fold, with both Sabre and Porter domains evident. It is therefore likely that the mechanotransmission mechanism also underpins extraction and transfer of lipoproteins from the inner membrane to the periplasmic LolA chaperone (33).

In the present study, we define the interaction between LolCDE and LolA using a combination of structural, biochemical and microbiological techniques. Atomic details of LolC-LolA interaction are captured by X-ray crystallography and the mode of binding is probed and validated using site-directed mutagenesis. We also analyse the nucleotide dependence of LolA binding to LolCDE and evaluate

existing biochemical data in context of the complete LolCDE model based on the structure of MacB. Our data provide fundamental insights into bacterial lipoprotein trafficking and may assist the development or improvement of existing Lol-pathway inhibitors.

Results

Structure of LolA bound to the periplasmic domain of LolC. We determined the crystal structure of LolA in complex with the periplasmic domain of LolC at 2 Å resolution. Crystals of the LolA·LolC complex belong to space group $P2_12_12$ and contain two complexes per asymmetric unit. Representative electron density for the LolA·LolC structure is shown in **Movie 1** and X-ray data and refinement statistics are given in **Table S1**. The buried surface area of the LolA·LolC complex is 1950 $Å^2$, which equates to 9 % of the total LolA surface.

The structure of LolA in complex with the periplasmic domain of LolC is shown in **Fig. 2*A***. The structures of isolated LolA (25) and the LolC periplasmic domain (33) have been described previously. LolA has a barrel-like fold comprised of an 11-stranded antiparallel β-sheet with a short helix located within its centre (25), and the LolC periplasmic domain shares its fold with the MacB ABC transporter (33). In the complex, LolC binds to LolA by means of a distinctive β-hairpin structure formed by residues P167-P179 (full-length LolC numbering) and a trio of surface residues (R163, Q181 and R182). We define the hairpin loop of LolC as the 'Hook' and the additional surface residues as the 'Pad'. The tip of the Hook constitutes a classical type I reverse-turn with M175 and P174 at its apex **(Fig. 2*B*)**. The tip residues make numerous hydrophobic interactions with LolA, including the side chains of F47, W49, L59, L66, L81, A84, F90, M91 and Y152. The backbone carbonyl of P174 forms a hydrogen bond with T88 of LolA. Hook residues F172, T173 and I178 also interact with residues in the LolA interior, but other residues in the Hook do not. The main chain of F172 is also involved in a hydrogen bonding network with Q22 and Q33 of LolA. The three residues of the Pad contribute to several intermolecular hydrogen bonds and R163 forms a salt bridge with D178 of LolA.

The conformation of LolC is not perturbed by interaction with LolA (root-mean-square deviation (rmsd) of 0.77Å over 224 residues). Conversely, as a consequence of the interaction with LolC, the LolA chaperone undergoes several conformational changes that are revealed by structural superposition of the LolA·LolC complex with known structures of LolA determined in isolation. **Figure S1** highlights four regions exhibiting large structural differences including per residue rmsd plots (**Fig. S1*A***), their mapping to the LolA structure (**Fig. S1*B***) and close-up structural comparisons (**Fig. S1*C*-*F***). A molecular morph of LolA transiting between LolC-bound and -free states is shown in **Movie 2**. The key differences in the structures are the widening of the mouth of LolA and

displacement of the central helix. Most structural displacements in LolA can be attributed to interactions with the LolC Hook (**Fig. S1*C*-*E***), but residues in the LolA C-terminus shift due to their interaction with the LolC Pad (**Fig. S1*F***).

The Hook and Pad of LolC are required for interaction with LolA. To assess the importance of the Hook and Pad in mediating complex formation between LolA and LolC, we made LolC periplasmic domain variants bearing point mutations in either the Hook or Pad and characterised their interaction with LolA using isothermal titration calorimetry (ITC) and size-exclusion chromatography (SEC). A representative ITC experiment for the interaction of LolA with wild-type LolC is presented in **Fig. 3*A*** with ITC data for the variants summarized in **Fig. 3*B*, *C***. The thermodynamic properties extracted from each ITC experiment are given in **Table S2** and example raw ITC data and fitted curves for each LolC variant are in **Fig. S2**. For wild-type LolC and LolA, we found that the complex is formed with high affinity (K_D 405 nM) and has a one-to-one stoichiometry. ITC also shows that complex formation is entropy-driven (ΔH 7.3 and $T\Delta S$ 16.0) confirming that hydrophobic interactions dominate the binding interface. Size-exclusion chromatography verifies complex formation between LolA and LolC, with an elution volume for LolA·LolC corroborating the equimolar stoichiometry of the crystal structure and ITC experiments (**Fig. 3*D***).

In contrast to the wild-type, a designed LolC protein construct lacking the Hook (LolC ΔHook) does not form a stable complex with LolA that is detectable by either ITC or SEC (**Fig. 3*B*, *D***). We solved the structure of this variant to demonstrate that the inability of LolC ΔHook to bind LolA is not due to loss of structural integrity (**Fig. S3*A***). Corresponding X-ray data and refinement statistics for the LolC ΔHook protein construct are given in **Table S1**, and a close-up of the electron density defining residues in the shortened loop is given in **Fig. S3*B***. LolC wild-type and ΔHook can be superposed with an rmsd of 0.57 Å for 207 matched Cα positions and inspection of the atomic coordinates reveals no obvious structural differences beyond the absence of the Hook itself (**Fig. S3*C***).

Having established the importance of the Hook for LolA binding, we next tested the relative importance of its constituent residues. Alanine substitutions of F172, M175, and R177 in the LolC Hook each give nearly 10-fold reductions in affinity for LolA, as measured by ITC (**Fig. 3*B*, *C*** & **Table S2**). T173A and I178A LolC variants are more substantially impaired (160-fold and 25-fold reductions) but the Q171A variant retains wild-type binding characteristics. The pattern of reduced affinity among alanine-substituted Hook variants correlates strongly with the reduction of favourable interactions between LolC and LolA expected from inspection of the LolA·LolC crystal structure. Residues F172, T173, M175 and I178 all make important contributions to the LolA-binding interface that would be diminished by alanine substitution while Q171 does not make meaningful contact with LolA. Reasons for impaired binding by the R177A variant are not clear as R177 does not contact

LolA, however, interactions between R177 and other LolC Hook residues (F172 and S170) suggest a probable role in maintaining Hook structure.

No individual alanine substitution in the Hook was sufficient to prevent binding of LolA to LolC, however an M175R variant lacks the capacity to bind LolA (**Fig. 3*B*, *C* & Table S2**). The location of M175 at the tip of the LolC Hook makes it a critical residue in the LolA·LolC interface, and substitution with arginine disrupts both the hydrophobic character and size of the Hook. The LolC M175R variant is stable and purified in similar yield to wild-type suggesting loss of LolA binding is due to steric hindrance and unfavourable electrostatics of the M175R substitution rather than protein misfolding.

The LolC Pad is significantly smaller than the Hook, but mutation of any of its three constituents (R163, Q181 and R182) reduces the affinity for LolA (**Fig. 3*B*, *C* & Table S2**). LolC Q181A and R182A variants exhibit 3- and 70-fold reductions in affinity, respectively. R163 is the most important Pad residue as the alanine variant is unable to bind LolA. Indeed, in the LolA·LolC crystal structure, R163 forms a salt bridge with D178 of LolA while Q181 and R163 support interfacial hydrogen bonds (**Fig. 2*B***). Overall, the ITC and SEC results demonstrate the importance of the LolC Hook and Pad in mediating interaction with LolA and highlight the roles of M175, T173, I178, R163 and R182 of LolC in the LolA·LolC heterodimer interface.

The Hook is conserved among LolC, LolE, and LolF proteins, but is absent from other ABC transporters belonging to the MacB ABC superfamily. To establish the generality of the Hook for interaction between LolC and LolA, we examined the amino acid sequences of LolC homologues. We found that a stretch of residues equivalent to the Hook is present in all LolC, LolE and LolF proteins analysed, but is absent from the MacB family of efflux pumps (including PvdT (40)) and the FtsEX cell division machinery (41, 42) (**Fig. 4*A***). Inspection of periplasmic domain structures for LolC, LolF, FtsX and MacB confirm that this result holds for all available structural data (**Fig. 4*B***). In conclusion, analysis of available homologous sequences and protein structures shows that the Hook is a conserved feature of lipoprotein trafficking machinery that is absent from other members of the Type VII ABC transporter superfamily.

The Hook in LolE does not support LolA binding. The conservation of a loop of residues in LolE at an equivalent position to the LolC Hook compelled us to test whether LolE is also able to bind LolA. We performed SEC and ITC experiments using a LolE periplasmic domain construct to assess potential LolA binding under the same conditions we observed binding to LolC. We found no evidence that LolA is able to bind the LolE periplasmic domain (**Fig. S5**). This result is consistent with previous work showing that *E. coli* LolC and LolE have different functions (27, 29), and suggests

the specific amino acid sequence of the LolC Hook is crucial for its interaction with LolA. Inspection of the LolE sequence reveals substantial sequence divergence in the Hook and absence of a residue equivalent to R163 of the LolC Pad despite clear retention of both Porter and Sabre subdomains. We conclude that the interaction between LolA and the LolCDE complex occurs exclusively through LolC and not with LolE, even though LolE is likely to possess the same overall fold as LolC.

LolC recognises features of LolA that are absent from LolB. LolA and LolB possess very similar protein folds (25) but it is not known how (or if) LolC is able to distinguish between these two proteins as binding partners. To address these questions, we evaluated the ability of soluble LolB to interact with the periplasmic domain of LolC by SEC (**Fig. S6*A***) and an IMAC-based pull-down assay (**Fig. S6*B***). We did not observe binding between LolC and LolB in either case - even though LolC is able to bind LolA under the same conditions. Relative to LolB, LolA has an extended C-terminus which is required for efficient LolA function (43). Our structure reveals that this C-terminal region contains the three residues, T176, D178 and Q180, that underpin interaction with the LolC Pad (**Figs. 2*B* & S6*C, D***). Sequence alignments confirm that the presence of a C-terminal extension is conserved among LolA proteins but absent from LolB (**Fig. S6*C*, *D***) suggesting that LolC does discriminate between LolA and LolB, and that interaction between the LolC Pad and the C-terminus of LolA is essential for chaperone recruitment to the LolCDE complex.

Structural determination of the F47E LolA variant reveals a domain-swapped dimer. Previous work has shown that an F47E LolA variant is defective in releasing lipoproteins from the bacterial inner membrane and tightly associates with proteoliposomes reconstituted with LolCDE (44). When expressed *in vivo*, F47E LolA impairs bacterial growth in a dominant negative fashion. Intrigued by the unusual phenotypic effects of the F47E LolA variant and its effect on the interaction of LolA and LolCDE, we further scrutinised this protein using biophysical methods.

We first measured association of the LolA F47E variant with LolC using ITC and found a >2-fold higher affinity of LolC for the F47E variant (K_D ~200 nM) compared to wild-type LolA (K_D ~405 nM) (**Fig. 5*A***). We then tried to rationalise this observation by inspecting the LolA·LolC crystal structure. The F47 side chain is located within the LolA interior (**Fig. 5*B***), and in the LolA·LolC complex is approximately 4 Å from M175 of LolC. A substitution of glutamate for phenylalanine at position 47 does not explain the higher affinity of the LolA variant for LolC because a polar residue would weaken otherwise favourable hydrophobic interactions with LolC. We therefore determined the crystal structure of the F47E variant (X-ray data and refinement statistics in **Table S1**). To our surprise, we found that the LolA F47E variant is a domain-swapped dimer (**Fig. 5*C*,** electron density in **Movie 3**). The N-terminal α-helix and first two β-strands from one monomer replace the equivalent elements in the other monomer and the substituting glutamate is shifted away from the LolA cavity into solvent.

The SEC elution profile of the F47E variant LolA confirms existence of the domain-swapped state in solution, although the peak is broader than that of the wild-type, and its apparent molecular weight (34 kDa) is smaller than expected from theory (46 kDa) (**Fig. 5*D***). Hypothesising that the domain-swapped state of the F47E variant may contribute to its unusual properties, we analysed the F47E structure for features that explain its enhanced affinity for LolC. Inspection revealed that the β-strand on which F47E is located is shifted approximately 6 Å relative to that of the wild-type (**Fig. 5*E***). The displacement of this strand affects the position of residues F47, W49, M51 and Q53- all of which face the LolA barrel interior, and two of which (F47 and W49) are involved in binding LolC in the wild-type protein. We therefore ascribe the 'tight-binding' properties of the F47E LolA variant to structural changes in the site that binds LolC resulting from a 'strand slip' induced by domain-swap dimerization.

In vivo **validation of the LolA·LolC interaction by mapping cross-link data.** We mapped the locations of LolA residues previously tested for their capacity to form photo-inducible crosslinks with LolCDE (27) to our crystal structure of the LolA·LolC complex (**Fig. 6*A***). A full list of the Tokuda lab's crosslinking results alongside nearest-neighbour distances measured from our crystal structure can be found in **Table S3**. There is excellent agreement between the *in vivo* crosslinking experiment and our crystal structure of the LolA·LolC complex. All seven LolA residues that crosslink to LolC are located within the binding interface (**Fig. 6*A*** *red*). Conversely, residues identified as ineffective in forming crosslinks are positioned in regions that do not contact LolC (**Fig. 6*A*** *blue*). The mapping of previous cross-linking data to our crystal structure of the LolA·LolC complex validates both approaches and confirms that the interface derived here by X-ray crystallography is representative of the state found *in vivo*.

Mutations in the Hook and Pad of LolC suppress dominant-negative *lolD* alleles. We re-examined data on previously reported LolC and LolE variants that suppress the dominant-negative effects of mutations in the LolCDE ATPase component, LolD (45). These mutants map primarily, though not exclusively, to periplasmic region of LolC and to the cytoplasmic domains of LolE, suggesting they provide relief from growth arrest by different mechanisms. Our structure shows that two of the suppressor mutations, P174S and G176R, are located within the Hook of LolC and another two, R182C and R182H, are based within the Pad (**Fig. 2*B***). Given the importance of the LolC Hook and Pad for LolA binding, our data predict that these four LolC periplasmic suppressors work by breaking the interaction between LolCDE and LolA to prevent accumulation of non-productive LolA·LolCDE complexes that otherwise lead to growth arrest. Putting these LolC suppressor mutations into a structural context highlights the importance of the Hook and Pad in mediating LolA recruitment by LolCDE, *in vivo*.

Disruption of the Lol system using knowledge of the LolA·LolC interaction. To further validate the interaction between LolA and LolC *in vivo*, we established an inducible plasmid-based system for expressing the LolC extracytoplasmic domain in the periplasm of *E. coli* with the intent of arresting growth through sequestration of LolA. Expression of the wild-type LolC extracytoplasmic domain in the periplasm produces growth arrest and cell lysis (**Fig. 6*B***). Conversely, expression of variants lacking the Hook, or with single amino acid substitutions in the Hook (M175R) or Pad (R163A) that have been shown to abrogate the interaction between LolA and LolC *in vitro*, do not lead to growth defects (**Fig. 6*B***) even though they are expressed at similar levels to the wild-type (**Fig. 6*C***). These observations are consistent with growth arrest resulting from sequestration of periplasmic LolA by the overexpressed wild-type LolC periplasmic domain construct that can be relieved by mutations disrupting favourable interactions between LolA and the LolC Hook and Pad.

LolA binding to LolCDE is mediated purely by access to the Hook and Pad and is independent of the ATP binding and hydrolysis cycle. To establish the behaviour of LolA binding within the context of the LolCDE complex, we immobilised detergent-purified LolCDE variants on Ni-IMAC resin and tested their ability to bind LolA. We also assayed each variant's ATPase activity using a spectrophotometric assay. Results are summarized for each variant in **Table 1** with the supporting data presented in **Figure S7**. We found that LolA binds to the wild-type LolCDE complex irrespective of the presence of nucleotide (**Table 1**, **Fig. S7*A, B***) and that LolCDE exhibits equivalent ATPase activity in the presence and absence of LolA (**Fig. S7*C*)**. Binding to LolA was also unaffected by mutation of a catalytic glutamate in LolD, or by the presence of a non-hydrolysable nucleotide analogue (ATPγS) (**Table 1**, **Fig. S7*A***). These results suggest that LolA binding to LolCDE is not dependent on the transporter nucleotide status, or its ability to hydrolyse ATP. Purified LolCDE complexes in which the LolC Hook was removed, or in which the Hook or Pad were disrupted maintain their ability to hydrolyse ATP, but are unable to bind LolA (**Table 1**, **Fig. S7*D*, *E***). In contrast, deletion of the Hook in LolE does not impair LolA-LolCDE interaction (**Table 1**, **Fig. S7*D***). We conclude that LolA binding to the LolCDE complex occurs exclusively through the Hook and Pad of LolC and is not regulated by nucleotide binding or hydrolysis.

Modelling of the LolA·LolCDE complex in ATP-bound and nucleotide-free states. Due to established homology (33), the structure of LolCDE (and its complex with LolA) can be modelled on the basis of available crystal structures of MacB, the LolC periplasmic domain, and the LolA·LolC complex. Such models are useful for contextualising the LolA-LolC interaction in three-dimensional space, giving clues as to the likely disposition of LolA relative to the membrane and other components of the LolCDE complex. We produced two distinct homology models of LolCDE corresponding to each of the different nucleotide states observed for the structural archetype of the family, MacB (33) (**Fig. 7**). The models show that binding of LolA to the LolCDE complex is feasible in both ATP-

bound and nucleotide-free states just as we found in our *in vitro* binding experiments (**Fig. S7**). The models also predict LolA to be located approximately 60 Å from the cytoplasmic membrane with the 'mouth' of the LolA barrel facing toward the LolE periplasmic domain. This result suggests that lipoproteins need not only be extracted from the inner membrane, but also passed a considerable distance to the waiting LolA chaperone on the top of LolCDE. While molecular details of lipoprotein transfer remain to be determined, the position and orientation of LolA are consistent with lipoprotein delivery via the central cavity between the periplasmic domains of LolC and LolE, perhaps aided by periplasmic conformational changes generated by mechanotransmission.

Inhibition of LolCDE by Compound 2 proceeds by mechanotransmission uncoupling. Homology models of LolCDE and LolA·LolCDE facilitate physical mapping of LolCDE mutations reported to provide resistance to two antimicrobial compounds: pyrrolopyrimidinedione 'G0507' (19) and pyridineimidazole 'Compound 2' (21) (hereon C2). G0507 and C2 are both purported inhibitors of LolCDE with potent antibacterial activity against *E. coli* strains lacking the tripartite efflux pump component, TolC. The majority of rescuing mutations for both G0507 and C2 cluster within the 'stalk' and 'shoulder' regions of the LolCDE complex, which are spatially close to one another despite separation in primary sequence (**Fig. 7, *right***). In MacB, stalk structure is intimately connected with mechanotransmission suggesting that G0507 and C2 exert their effects by interfering with analogous movements necessary for coupling LolCDE's cytoplasmic ATPase activity with the lipoprotein transfer reaction. Consistent with this 'mechanotransmission uncoupling' as a hypothesis for the action of these inhibitors, G0507 is known to stimulate ATPase activity of LolCDE while inhibiting the release of lipoproteins from the inner membrane (19). Since C2 also inhibits lipoprotein release, we tested its effect on LolCDE ATPase activity and found that, like G0507, C2 causes an increase in the rate of hydrolysis (**Fig. S8*A***). We also found that C2 does not have any detectable effect on LolA binding to the LolC periplasmic domain nor LolCDE, as judged by IMAC-based pull-down experiments, ruling out competition between the inhibitor and the chaperone as an alternative hypothesis (**Fig. S8*B*, *C***).

Discussion

We solved the crystal structure of the periplasmic lipoprotein chaperone, LolA, in complex with the extracytoplasmic domain of LolC (**Fig. 2**). LolC recruits LolA by means of a finger-like protrusion that we term the Hook and a patch of surface residues termed the Pad. Isothermal titration calorimetry and size-exclusion chromatography, coupled with structure-led amino acid substitutions in LolC, demonstrate the importance of these features (**Fig. 3**) and sequence-based analyses show that the Hook is conserved among LolC proteins but absent from homologous ABC transporters (such as MacB, PvdT and FtsEX) that do not have a lipoprotein trafficking function (**Fig. 4**). We uncovered the

structural basis for enhanced affinity of the LolA F47E variant (**Fig. 5**) and validated the native LolA·LolC interface *in vivo* using crosslinking data from the Tokuda lab and a growth inhibition assay (**Fig. 6**). The interaction between LolC and LolA was confirmed for the detergent-purified LolCDE complex and was demonstrated to be independent of nucleotide binding and hydrolysis (**Table 1**). Modelling of LolCDE based on crystal structures of the MacB ABC transporter and LolC periplasmic domain predicts the likely structural context of the LolA-LolC interaction and implicates mechanotransmission in lipoprotein extraction and delivery to LolA (**Fig. 7**). The location of mutations that rescue LolCDE from the chemical inhibitors further suggest such compounds work by interfering directly with mechanotransmission, effectively uncoupling cytoplasmic ATP hydrolysis from periplasmic conformational changes necessary to drive lipoprotein transfer. The combined data give essential mechanistic insights into the progression of lipoproteins from inner membrane to the periplasmic LolA chaperone during lipoprotein trafficking.

The key features of LolC that underpin binding of LolA are the Hook and Pad. Disruption of either causes substantial reduction in the affinity of LolA for LolC and complex formation is abrogated entirely if the Hook is deleted or if R163 of the Pad is replaced with alanine. These experiments demonstrate that the binding interface of LolC is bipartite and that neither Hook nor Pad alone is sufficient to mediate interaction with LolA. Comparison of the structure of the LolA·LolC complex with that of LolA in isolation reveals significant conformational changes that suggest it may represent a 'receptive state' for lipoprotein binding. Several studies implicate the 'mouth' of the LolA barrel as a putative site for lipoyl group interaction (25, 27, 46, 47) meaning that both the Hook and lipoprotein may be in competition for the same binding site. If so, it is plausible that lipoprotein binding to LolA may directly cause release from LolC by displacement of the Hook.

The work presented here establishes the interaction of LolA with LolC as independent of ATP binding and hydrolysis by the LolCDE complex. A key question for LolCDE, therefore, is what the role of energy input is, *in vivo*. Given nucleotide cycling is not required for LolA binding, the most likely role for ATP binding and hydrolysis is in driving lipoprotein extraction from the inner membrane. Efforts to determine the role of ATP binding and hydrolysis in the release of lipoproteins from LolCDE have been made previously (48, 49), but molecular details of this process remain obscure. One possibility is that ATP-powered extraction of lipoproteins from the inner membrane by the LolCDE complex uses a mechanotransmission mechanism as described for MacB (33). ATP-bound and nucleotide-free states of MacB have been structurally characterised, revealing long-range conformational changes and extensive periplasmic motions driven by ATP binding and hydrolysis. Similar motions in the LolCDE complex may provide the mechanical force needed to 'pull' the lipoprotein from the inner membrane.
Our structural model suggests that LolA is bound as much as 60 Å from the inner membrane surface. Previous work has shown that LolE is the site of lipoprotein binding (29), but fine details of where the

interface is located are yet to be determined. Mechanotransmission-driven parting of the periplasmic domains in LolCDE might expose an intermediate lipoprotein binding site between LolC and LolE periplasmic domains that would provide a 'stop-off point' between the membrane and chaperone. Additional experiments will be required to test these hypotheses further.

In summary, we have determined the crystal structure of LolA in complex with the periplasmic domain of LolC and probed the physical basis of the interaction using complementary techniques. We find that complex formation between LolA and LolC is independent of the LolCDE ATP binding and hydrolysis cycle and propose a mechanism where recruitment of LolA to the LolC Hook facilitates presentation to newly-extracted lipoproteins, possibly pulled from the membrane in an ATP-dependent manner by a mechanotransmission mechanism resembling that of the MacB ABC transporter.

Methods

Complete **Supplemental Methods** are available to download. In brief, structures of LolA bound to the LolC periplasmic domain, the LolA F47E variant, and LolC ΔHook periplasmic domain were each determined by X-ray crystallography. Proteins were expressed in *E. coli*, purified using Ni-based immobilised metal affinity chromatography (Ni-IMAC) and crystallised using a sitting drop vapour diffusion setup. Crystals of the LolA·LolC complex were obtained in 100 mM HEPES pH 6.5 and 45 % (w/v) poly(acrylic acid) 2100. LolA F47E was crystallised in 13 % (w/v) PEG 8000, 20 % (v/v) glycerol. The periplasmic domain of LolC ΔHook was crystallised in 30 % (w/v) PEG 2000 MME, 200 mM ammonium sulfate, 150 mM sodium acetate pH 4.6, assisted by seeds from crystals of the wild-type LolC periplasmic domain obtained previously (33). Crystals were cryoprotected prior to flash freezing in liquid nitrogen using the reservoir solution supplemented with either 20 % ethylene glycol (LolA·LolC) or 25 % (v/v) glycerol (LolC ΔHook and LolA F47E). X-ray diffraction data were collected remotely at ESRF (France) and Diamond (UK) synchrotrons. Structure determinations used the CCP4 suite (50). Diffraction data were indexed and reduced with iMOSFLM (51), scaled with Aimless (52) and phased by molecular replacement using Phaser (53). Probes for molecular replacement were derived from PDB entries, 5NAA (33) and 1IWL (25). Model building and refinement used Coot (54) and Refmac (55). Structure validation was assisted by RAMPAGE (56) and Procheck (57). Size-Exclusion Chromatography (SEC) was performed using an Äkta FPLC equipped with a Superdex 75, 10/300 GL column. Typically, 100 µL of protein at 200 µM was analysed. Isothermal Titration Calorimetry (ITC) experiments were performed using a Microcal VP-ITC instrument. A typical titration used LolA in the cell (25 µM) and LolC variant in the syringe (300 or 450 µM) with 30 x 10 µL-injections (reference power 25, 300 rpm stirring, 25 °C). LolA binding to His-tagged LolC periplasmic domain or LolCDE immobilised on IMAC resin was performed using microbatch spin columns. Immobilised proteins were incubated with tag-free LolA for ~5 min, washed three times, then eluted and visualised by SDS-PAGE. ATPase activity of purified LolCDE variants

was assessed using the EnzChek phosphate assay kit (Thermofisher) at 1 μM concentration. Purified LolCDE variants used dodecyl maltopyranoside as a stabilising detergent. The growth-inhibitory effect of extracytoplasmic targeting of the LolC periplasmic domain was assessed by monitoring OD_{600} of *E. coli* C43 (DE3) cultures (58) expressing the wild-type or variant domain fused behind an N-terminal Sec secretion signal.

Acknowledgements

We gratefully acknowledge the gift of LolCDE inhibitor, Compound 2, from Entasis Therapeutics. We thank staff at ESRF (France) and Diamond (UK) synchrotrons for beamline facilities. This work was supported by grants from the UK Medical Research Council (MR/N000994/1) and the Wellcome Trust (101828/Z/13/Z).

Author contributions

E.K., N.P.G., A.C., and V.K. designed research, performed research, analysed data, and wrote the paper.

References

1. Konovalova A, Kahne DE, Silhavy TJ (2017) Outer Membrane Biogenesis. *Annu Rev Microbiol* 71(1):539–556.
2. Henderson JC, et al. (2016) The Power of Asymmetry: Architecture and Assembly of the Gram-Negative Outer Membrane Lipid Bilayer. *Annu Rev Microbiol* 70(1):255–278.
3. Braun V, Rehn K (1969) Chemical Characterization, Spatial Distribution and Function of a Lipoprotein (Murein-Lipoprotein) of the *E. coli* Cell Wall. The Specific Effect of Trypsin on the Membrane Structure. *Eur J Biochem* 10(3):426–438.
4. Cascales E, Bernadac A, Gavioli M, Lazzaroni J-C, Lloubes R (2002) Pal lipoprotein of *Escherichia coli* plays a major role in outer membrane integrity. *J Bacteriol* 184(3):754–9.
5. Gu Y, et al. (2016) Structural basis of outer membrane protein insertion by the BAM complex. *Nature* 531(7592):64–69.
6. Noinaj N, Gumbart JC, Buchanan SK (2017) The β-barrel assembly machinery in motion. *Nat Rev Microbiol* 15(4):197–204.
7. Qiao S, Luo Q, Zhao Y, Zhang XC, Huang Y (2014) Structural basis for lipopolysaccharide insertion in the bacterial outer membrane. *Nature* 511(7507):108–111.
8. Dong H, et al. (2014) Structural basis for outer membrane lipopolysaccharide insertion. *Nature* 511(7507):52–56.
9. Malinverni JC, Silhavy TJ (2009) An ABC transport system that maintains lipid asymmetry in

the gram-negative outer membrane. *Proc Natl Acad Sci U S A* 106(19):8009–14.

10. Abellón-Ruiz J, et al. (2017) Structural basis for maintenance of bacterial outer membrane lipid asymmetry. *Nat Microbiol* 2(12):1616–1623.

11. Typas A, et al. (2010) Regulation of Peptidoglycan Synthesis by Outer-Membrane Proteins. *Cell* 143(7):1097–1109.

12. Grabowicz M, Silhavy TJ (2017) Redefining the essential trafficking pathway for outer membrane lipoproteins. *Proc Natl Acad Sci U S A* 114(18):4769–4774.

13. Yakushi T, Tajima T, Matsuyama S, Tokuda H (1997) Lethality of the Covalent Linkage between Mislocalized Major Outer Membrane Lipoprotein and the Peptidoglycan of *Escherichia coli*. *J Bacteriol* 179(9):2857–2862.

14. Matsuyama S-I, Yokota N, Tokuda H (1997) A novel outer membrane lipoprotein, LolB (HemM), involved in the LolA (p20)-dependent localization of lipoproteins to the outer membrane of *Escherichia coli*. *EMBO J* 16(23):6947–6955.

15. Tajima T, Yokota N, Matsuyama S, Tokuda H (1998) Genetic analyses of the in vivo function of LolA, a periplasmic chaperone involved in the outer membrane localization of *Escherichia coli* lipoproteins. *FEBS Lett* 439(1–2):51–54.

16. Tanaka K, Matsuyama SI, Tokuda H (2001) Deletion of lolB, encoding an outer membrane lipoprotein, is lethal for *Escherichia coli* and causes accumulation of lipoprotein localization intermediates in the periplasm. *J Bacteriol* 183(22):6538–42.

17. Narita S, Tanaka K, Matsuyama S, Tokuda H (2002) Disruption of lolCDE, encoding an ATP-binding cassette transporter, is lethal for *Escherichia coli* and prevents release of lipoproteins from the inner membrane. *J Bacteriol* 184(5):1417–22.

18. Buddelmeijer N (2015) The molecular mechanism of bacterial lipoprotein modification—How, when and why? *FEMS Microbiol Rev* 39(2):246–261.

19. Nickerson NN, et al. (2018) A novel inhibitor of the LolCDE ABC transporter essential for lipoprotein trafficking in Gram-negative bacteria. *Antimicrob Agents Chemother*:AAC.02151-17.

20. Nayar AS, et al. (2015) Novel antibacterial targets and compounds revealed by a high-throughput cell wall reporter assay. *J Bacteriol* 197(10):1726–34.

21. McLeod SM, et al. (2015) Small-molecule inhibitors of gram-negative lipoprotein trafficking discovered by phenotypic screening. *J Bacteriol* 197(6):1075–82.

22. Okuda S, Tokuda H (2011) Lipoprotein Sorting in Bacteria. *Annu Rev Microbiol* 65(1):239–259.

23. Masuda K, Matsuyama S, Tokuda H (2002) Elucidation of the function of lipoprotein-sorting signals that determine membrane localization. *Proc Natl Acad Sci U S A* 99(11):7390–5.

24. Yakushi T, Masuda K, Narita S, Matsuyama S, Tokuda H (2000) A new ABC transporter mediating the detachment of lipid-modified proteins from membranes. *Nat Cell Biol* 2(4):212–

218.
25. Takeda K, et al. (2003) Crystal structures of bacterial lipoprotein localization factors, LolA and LolB. *EMBO J* 22(13):3199–209.
26. Tsukahara J, Mukaiyama K, Okuda S, Narita S, Tokuda H (2009) Dissection of LolB function - lipoprotein binding, membrane targeting and incorporation of lipoproteins into lipid bilayers. *FEBS J* 276(16):4496–4504.
27. Okuda S, Tokuda H (2009) Model of mouth-to-mouth transfer of bacterial lipoproteins through inner membrane LolC, periplasmic LolA, and outer membrane LolB. *Proc Natl Acad Sci U S A* 106(14):5877–82.
28. Nakada S, et al. (2009) Structural investigation of the interaction between LolA and LolB using NMR. *J Biol Chem* 284(36):24634–24643.
29. Mizutani M, et al. (2013) Functional differentiation of structurally similar membrane subunits of the ABC transporter LolCDE complex. *FEBS Lett* 587(1):23–29.
30. LoVullo ED, Wright LF, Isabella V, Huntley JF, Pavelka MS (2015) Revisiting the Gram-negative lipoprotein paradigm. *J Bacteriol* 197(10):1705–15.
31. Wang B, Dukarevich M, Sun EI, Yen MR, Saier MH (2009) Membrane Porters of ATP-Binding Cassette Transport Systems Are Polyphyletic. *J Membr Biol* 231(1):1–10.
32. Khwaja M, Ma Q, Saier MH (2005) Topological analysis of integral membrane constituents of prokaryotic ABC efflux systems. *Res Microbiol* 156(2):270–277.
33. Crow A, Greene NP, Kaplan E, Koronakis V (2017) Structure and mechanotransmission mechanism of the MacB ABC transporter superfamily. *Proc Natl Acad Sci U S A* 114(47):12572–12577.
34. Kobayashi N, Nishino K, Yamaguchi A (2001) Novel macrolide-specific ABC-type efflux transporter in *Escherichia coli*. *J Bacteriol* 183(19):5639–44.
35. Yamanaka H, Kobayashi H, Takahashi E, Okamoto K (2008) MacAB is involved in the secretion of *Escherichia coli* heat-stable enterotoxin II. *J Bacteriol* 190(23):7693–7698.
36. Okada U, et al. (2017) Crystal structure of tripartite-type ABC transporter MacB from *Acinetobacter baumannii*. *Nat Commun* 8(1):1336.
37. Fitzpatrick AWP, et al. (2017) Structure of the MacAB–TolC ABC-type tripartite multidrug efflux pump. *Nat Microbiol* 2:17070.
38. Greene NP, Kaplan E, Crow A, Koronakis V (2018) Antibiotic Resistance Mediated by the MacB ABC Transporter Family: A Structural and Functional Perspective. *Front Microbiol* 9:950.
39. Yasuda M, Iguchi-Yokoyama A, Matsuyama S, Tokuda H, Narita S (2009) Membrane Topology and Functional Importance of the Periplasmic Region of ABC Transporter LolCDE. *Biosci Biotechnol Biochem* 73(10):2310–2316.
40. Imperi F, Tiburzi F, Visca P (2009) Molecular basis of pyoverdine siderophore recycling in

Pseudomonas aeruginosa. *Proc Natl Acad Sci U S A* 106(48):20440–20445.
41. Yang DC, et al. (2011) An ATP-binding cassette transporter-like complex governs cell-wall hydrolysis at the bacterial cytokinetic ring. *Proc Natl Acad Sci* 108(45):E1052–E1060.
42. Mavrici D, et al. (2014) *Mycobacterium tuberculosis* FtsX extracellular domain activates the peptidoglycan hydrolase, RipC. *Proc Natl Acad Sci U S A* 111(22):8037–42.
43. Okuda S, Watanabe S, Tokuda H (2008) A short helix in the C-terminal region of LolA is important for the specific membrane localization of lipoproteins. *FEBS Lett* 582(15):2247–2251.
44. Miyamoto A, Matsuyama S, Tokuda H (2002) Dominant negative mutant of a lipoprotein-specific molecular chaperone, LolA, tightly associates with LolCDE. *FEBS Lett* 528(1–3):193–196.
45. Ito Y, Matsuzawa H, Matsuyama S, Narita S, Tokuda H (2006) Genetic analysis of the mode of interplay between an ATPase subunit and membrane subunits of the lipoprotein-releasing ATP-binding cassette transporter LolCDE. *J Bacteriol* 188(8):2856–64.
46. Oguchi Y, et al. (2008) Opening and closing of the hydrophobic cavity of LolA coupled to lipoprotein binding and release. *J Biol Chem* 283(37):25414–20.
47. Watanabe S, Oguchi Y, Takeda K, Miki K, Tokuda H (2008) Introduction of a lethal redox switch that controls the opening and closing of the hydrophobic cavity in LolA. *J Biol Chem* 283(37):25421–7.
48. Ito Y, Kanamaru K, Taniguchi N, Miyamoto S, Tokuda H (2006) A novel ligand bound ABC transporter, LolCDE, provides insights into the molecular mechanisms underlying membrane detachment of bacterial lipoproteins. *Mol Microbiol* 62(4):1064–1075.
49. Taniguchi N, Tokuda H (2008) Molecular events involved in a single cycle of ligand transfer from an ATP binding cassette transporter, LolCDE, to a molecular chaperone, LolA. *J Biol Chem* 283(13):8538–44.
50. Winn MD, et al. (2011) Overview of the CCP4 suite and current developments. *Acta Crystallogr Sect D Biol Crystallogr* 67:235–242.
51. Battye TGG, Kontogiannis L, Johnson O, Powell HR, Leslie AGW (2011) iMOSFLM: A new graphical interface for diffraction-image processing with MOSFLM. *Acta Crystallogr Sect D Biol Crystallogr* 67:271–281.
52. Evans PR, Murshudov GN (2013) How good are my data and what is the resolution? *Acta Crystallogr Sect D Biol Crystallogr* 69(7):1204–1214.
53. McCoy AJ, et al. (2007) Phaser crystallographic software. *J Appl Crystallogr* 40(4):658–674.
54. Emsley P, Lohkamp B, Scott WG, Cowtan K (2010) Features and development of Coot. *Acta Crystallogr Sect D Biol Crystallogr* 66:486–501.
55. Murshudov GN, et al. (2011) REFMAC5 for the refinement of macromolecular crystal structures. *Acta Crystallogr Sect D Biol Crystallogr* 67:355–367.

587 56. Lovell SC, et al. (2003) Structure validation by C alpha geometry: phi,psi and C beta deviation.
588 *Proteins-Structure Funct Genet* 50(3):437–450.
589 57. Laskowski RA, MacArthur MW, Moss DS, Thornton JM (1993) PROCHECK: a program to
590 check the stereochemical quality of protein structures. *J Appl Crystallogr* 26(2):283–291.
591 58. Miroux B, Walker JE (1996) Over-production of Proteins in *Escherichia coli*: Mutant Hosts
592 that Allow Synthesis of some Membrane Proteins and Globular Proteins at High Levels. *J Mol*
593 *Biol* 260(3):289–298.
594 59. Guzman LM, Belin D, Carson MJ, Beckwith J (1995) Tight regulation, modulation, and high-
595 level expression by vectors containing the arabinose PBAD promoter. *J Bacteriol*
596 177(14):4121–30.
597 60. Cowtan K (2010) Recent developments in classical density modification. *Acta Crystallogr Sect*
598 *D Biol Crystallogr* 66:470–478.
599 61. Cowtan K (2006) The Buccaneer software for automated model building. 1. Tracing protein
600 chains. *Acta Crystallogr Sect D Biol Crystallogr* 62:1002–1011.
601 62. Kelley LA, Mezulis S, Yates CM, Wass MN, Sternberg MJE (2015) The Phyre2 web portal for
602 protein modeling, prediction and analysis. *Nat Protoc* 10(6):845–858.
603 63. Pei J, Kim B-H, Grishin N V. (2008) PROMALS3D: a tool for multiple protein sequence and
604 structure alignments. *Nucleic Acids Res* 36(7):2295–2300.
605

Figures

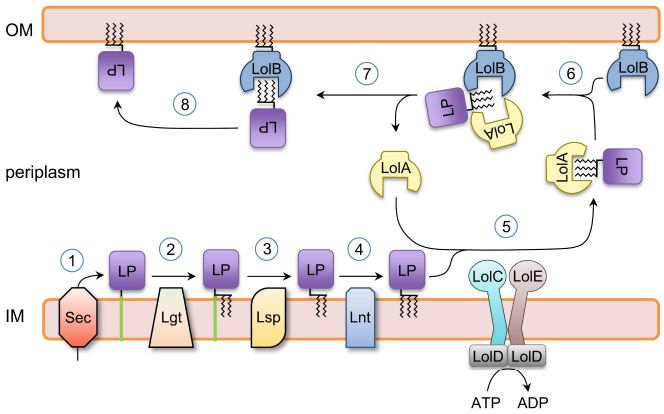

Figure 1. Lipoprotein maturation and trafficking in *E. coli*. Steps 1-8 show a generic lipoprotein (LP) undergoing maturation and transport to the bacterial outer membrane (OM). (1) Immature lipoprotein is secreted by the Sec system and integrated in the inner membrane (IM). (2) Lgt adds diacylglycerol to the lipobox cysteine residue. (3) Lsp removes the transmembrane signal peptide. (4) Lnt acylates the lipoprotein N-terminus amino group. (5) LolCDE transfers the mature (triacylated) lipoprotein to the LolA chaperone. (6) Lipoprotein is passed from LolA to LolB by a 'mouth-to-mouth' mechanism. (7) LolA is recycled, leaving lipoprotein bound to LolB. (8) LolB releases lipoprotein to the outer membrane.

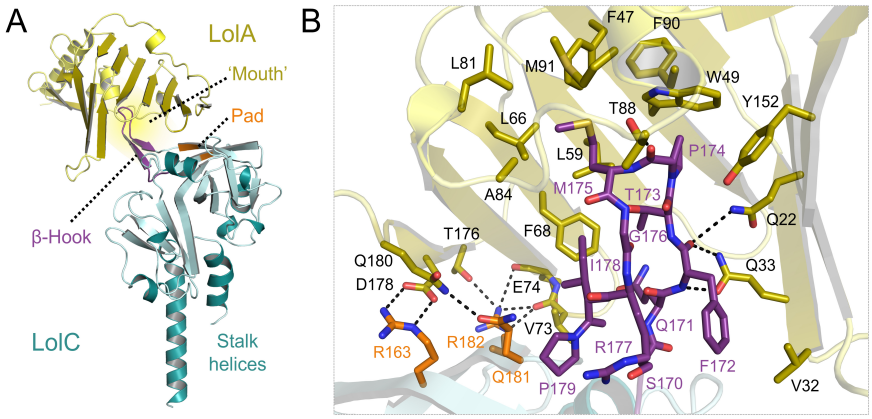

Figure 2. Crystal structure of LolA bound to LolC periplasmic domain. (A) Overall structure of the LolA·LolC complex. (B) Close-up view of the interaction interface. LolC and LolA are shown in *cyan* and *gold*, respectively. LolC residues belonging to the Hook and the Pad are shown in *purple* and *orange*. LolA residues interacting with LolC are shown in stick representation.

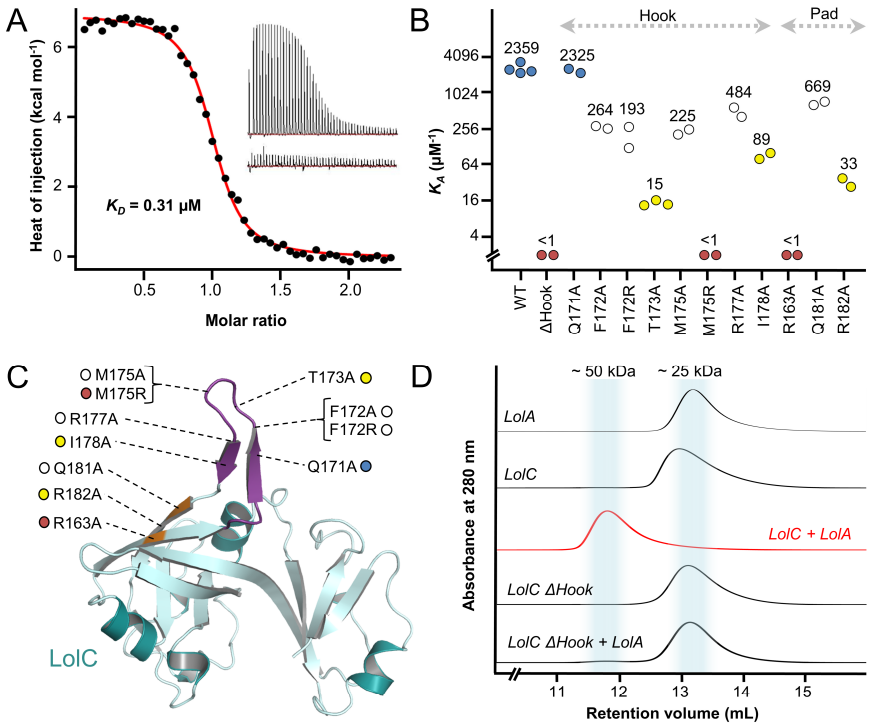

Figure 3. Isothermal titration calorimetry (ITC) and size-exclusion chromatography (SEC) experiments probing the LolA·LolC interface. (A) Representative ITC experiment demonstrating interaction between LolA and LolC. The main figure shows background-corrected heats of injection and a fitted binding curve (*red*). The two thermograms underpinning this curve are shown inset: injection of LolC into a cell containing LolA (*top*) and injection of LolC into buffer (*bottom*). (B) Association constants (K_A) for wild-type and variant LolC periplasmic domains with LolA determined using ITC. Median values (μM^{-1}) are indicated above each cluster of repeat experiments. Colouring is used to categorise binding strength of variants: wild-type-like binding, *blue*; modestly impaired, *white*; strongly impaired, *yellow* and non-binders, *red*. (C) Locations of amino acid substitutions in context of the LolC periplasmic domain (Hook *purple* and Pad *orange*). (D) SEC profiles for indicated proteins.

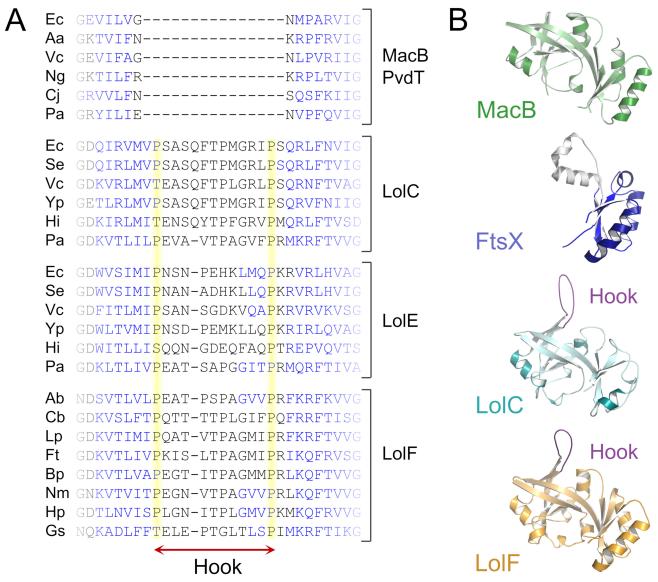

Figure 4. Structural and bioinformatic evidence that the Hook is conserved among LolC, LolE and LolF but absent from the wider Type VII ABC Transporter superfamily. (A) Multiple sequence alignment comparing Lol-family proteins (LolC, LolE and LolF) with MacB and PvdT in the region of the Hook. Proline residues flanking the Hook are highlighted in *yellow*, and predicted β-sheets in *blue*. The full multiple sequence alignment is provided in **Figure S4**. Abbreviations are as follows: Ec, *Escherichia coli*; Aa, *Aggregatibacter actinomycetemcomitans*; Vc, *Vibrio cholerae*; Ng, *Neisseria gonorrhoeae*; Cj, *Campylobacter jejuni*; Pa, *Pseudomonas aeruginosa*; Se, *Salmonella enterica* serovar Typhimurium; Yp, *Yersinia pestis*; Hi, *Haemophilus influenzae*; Ab, *Acinetobacter baumannii*; Cb, *Coxiella burnetii*; Lp, *Legionella pneumophila*; Ft, *Francisella tularensis*; Bp, *Burkholderia pseudomallei*; Nm, *Neisseria meningitidis*; Hp, *Helicobacter pylori*; Gs, *Geobacter sulfurreducens*. (B) Comparison of the periplasmic domains of *A. actinomycetemcomitans* MacB (5LIL), *Mycobacterium tuberculosis* FtsX (4N8N), *E. coli* LolC (5NAA) and *A. baumannii* LolF (5UDF, annotated as LolE in the PDB). LolC and LolF Hooks are shown in *purple*. FtsX lacks a Sabre domain, the remaining Porter is shown in *blue* and pair of helices at the location of the missing Sabre in *grey*.

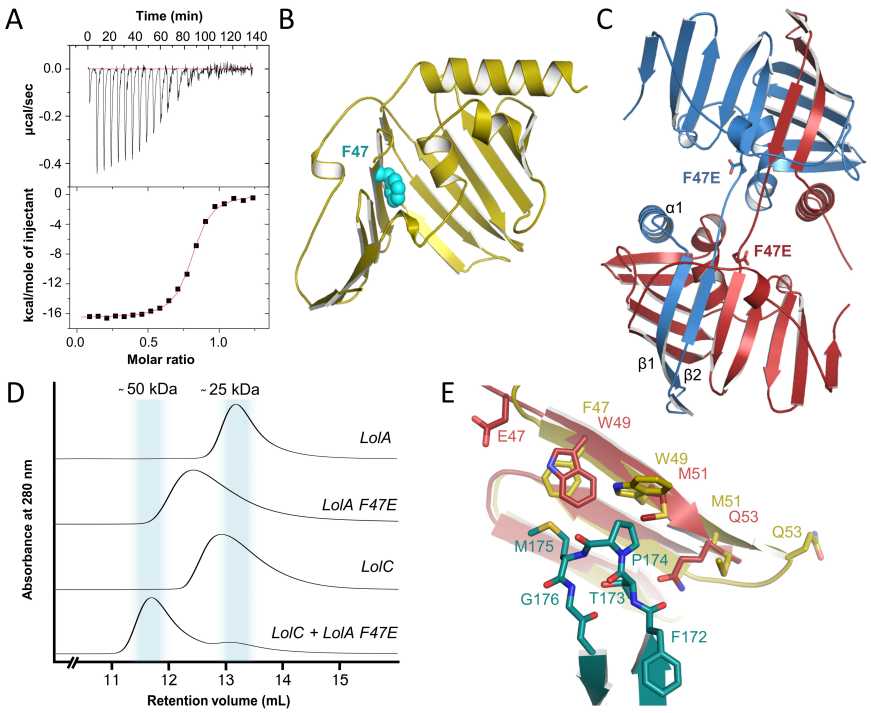

Figure 5. Structural and functional analysis of the 'tight-binding' LolA F47E variant. (A) ITC experiment demonstrating binding of LolA F47E to the LolC periplasmic domain. (B) Location of residue F47 in wild-type LolA. (C) Crystal structure of LolA F47E revealing a domain-swapped dimer. (D) Size-exclusion chromatography experiment for wild-type and LolA F47E variant. (E) Close-up view of LolA F47E variant showing the strand-slip affecting the location of residues E/F47, W49, M51 and Q53. LolA wild-type and F47E are in *yellow* and *red* respectively, LolC Hook shown in *teal*.

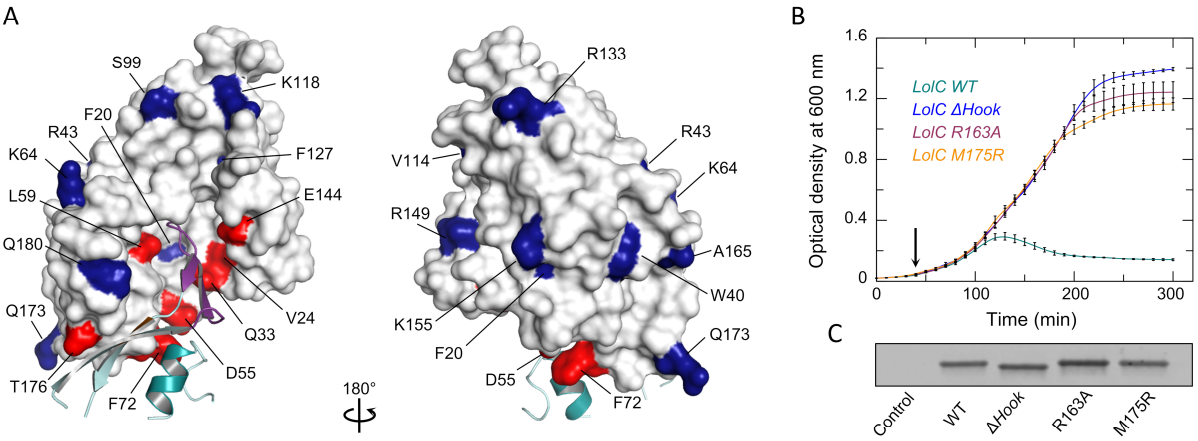

677
678

679 **Figure 6. *In vivo* validation of the LolA·LolC complex.** (A) LolA positions determined to interact
680 with LolC by *in vivo* crosslinking (27) mapped onto the LolA·LolC structure. LolC is represented in
681 *cyan* with the Hook in *purple*. LolA is shown as a solid surface, residues reported to form crosslinks to
682 LolC are coloured *red*, and those that do not are *blue*. (B) Growth curves for *E. coli* C43 (DE3) cells
683 expressing the extracytoplasmic domain of wild-type LolC (or indicated variant) with a periplasmic
684 targeting sequence. Protein expression was induced with 0.2 % arabinose at the time point indicated
685 by an arrow. Curves depict the mean ± standard deviation for three independent cultures. (C)
686 Immunoblot showing expression level of periplasmic extracts from *E. coli* C43 (DE3) cells bearing
687 empty vector (Control), or expressing the extracytoplasmic domain of wild-type LolC (WT) or
688 indicated variant.

689
690

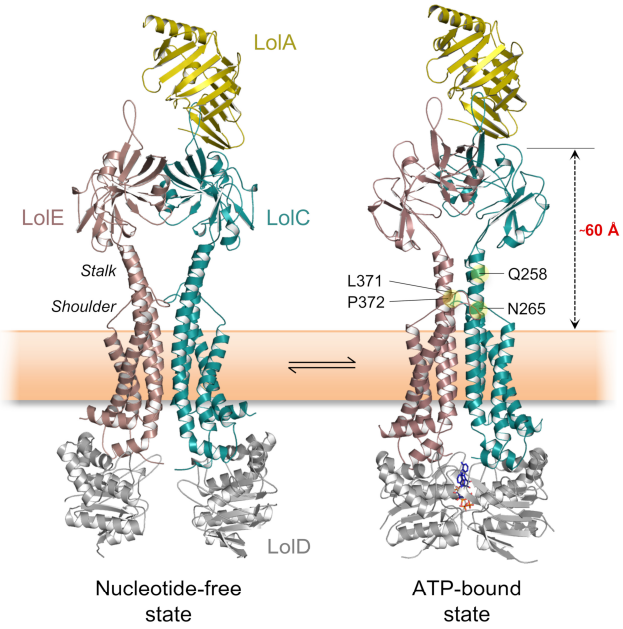

Figure 7. Homology-based models of the LolA·LolCDE complex. Models of full-length LolCDE generated from the nucleotide-free and ATP-bound structures of MacB (5NIL and 5LIL respectively). LolA has been docked according to LolA·LolC crystallographic data (6F3Z). Positions at which mutations confer resistance to both Compound 2 (21) and G0507 inhibitors (19) are shown mapped to the ATP-bound state.

Supplementary Information

Insights into bacterial lipoprotein trafficking from a structure of LolA bound to the LolC periplasmic domain

Elise Kaplan, Nicholas P. Greene, Allister Crow [‡], *Vassilis Koronakis* *

Department of Pathology, University of Cambridge, UK.

[‡] Current address: School of Life Sciences, University of Warwick, UK.

***Corresponding author: vk103@cam.ac.uk**

Supplementary information includes:

Figs. S1 to S9
Tables S1 to S5
Supplementary methods
Captions for movies 1 to 3

Other supplementary materials for this manuscript:

Movies 1 to 3

Supplemental Figures

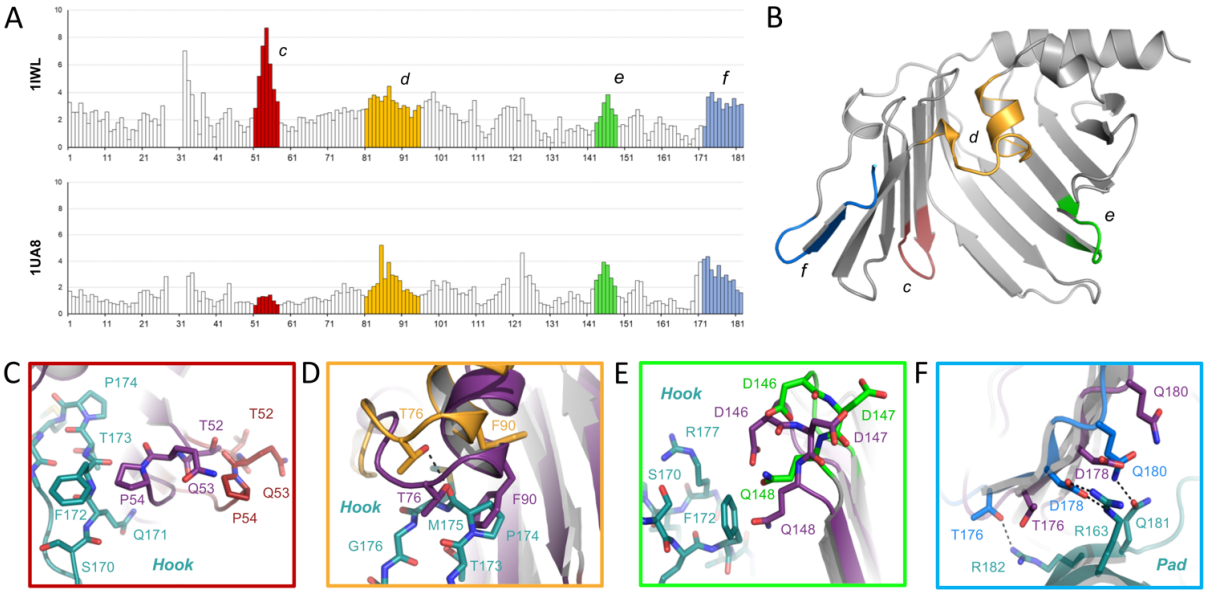

Figure S1. Comparison of LolA in isolation and in complex with LolC. (A) Rmsd plots for superpositions of LolA in complex with LolC (6F3Z) with structures of LolA in isolation (1IWL and 1UA8). Four regions with significant conformational differences are highlighted. (B) Structure of LolA colour-coded as per the rmsd plot. (C-F) Close-up views of LolA conformational differences in each region. Isolated LolA (1IWL) is shown in *purple* and the LolA·LolC complex is shown with LolC in *teal* and LolA coloured as in (B).

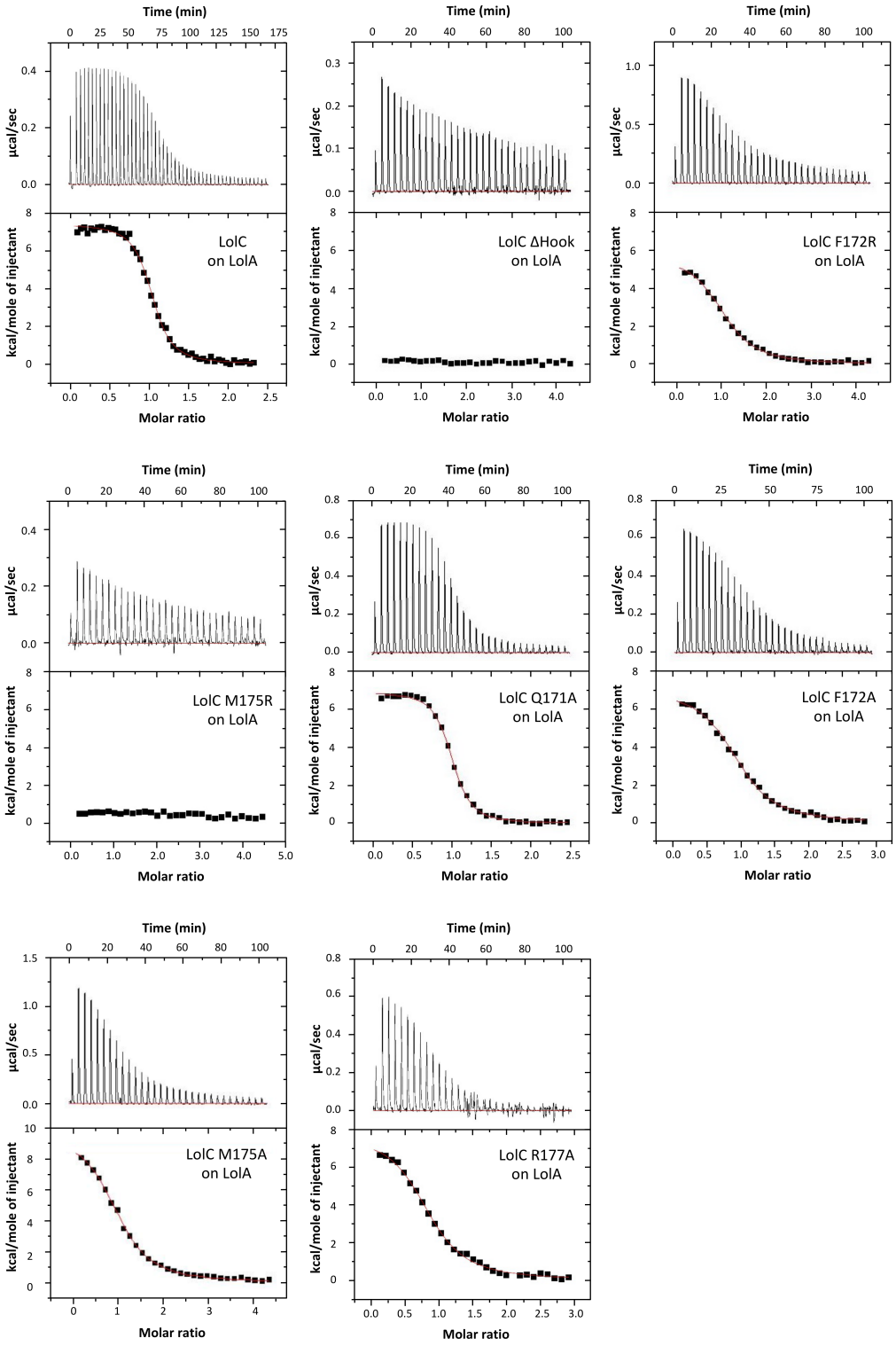

Figure S2. ITC titrations for LolA using wild-type or variant LolC periplasmic domain constructs. For each titration, a representative thermogram is shown in the upper part of the panel and fitted plot of background-subtracted heats of injection is shown immediately beneath. Values of affinities and thermodynamic parameters for all repeats are given in **Table S2**.

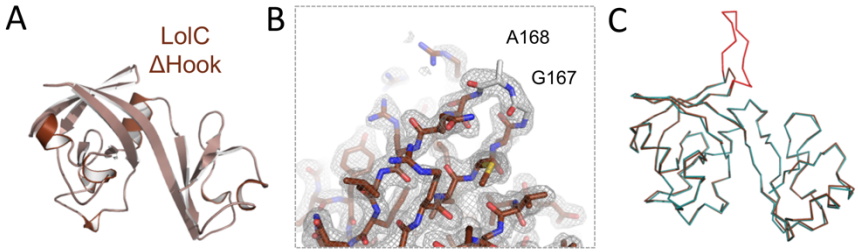

Figure S3. Removing the Hook from LolC does not disrupt its structure. (A) Crystal structure of the LolC ΔHook periplasmic domain construct. (B) Close-up view of the LolC ΔHook structure showing electron density for the linker residues (*light grey*) replacing the truncated Hook and surrounding β-strands. The mesh represents a weighted $2|F_o|-|F_c|$ electron density map contoured at 1 sigma. (C) Alignment of LolC ΔHook (*brown*) and wild-type periplasmic domains (*teal*). Hook shown in *red*.

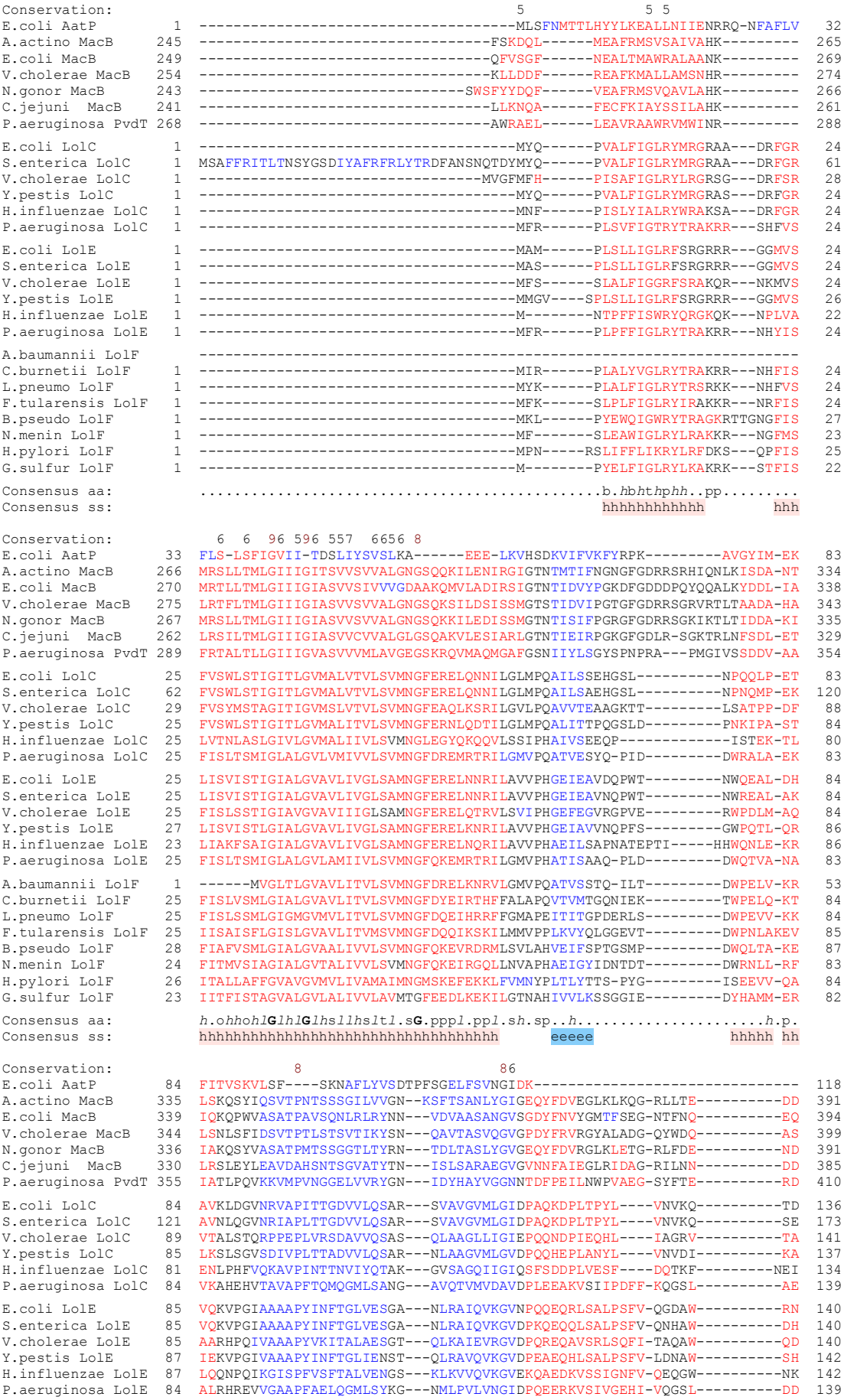

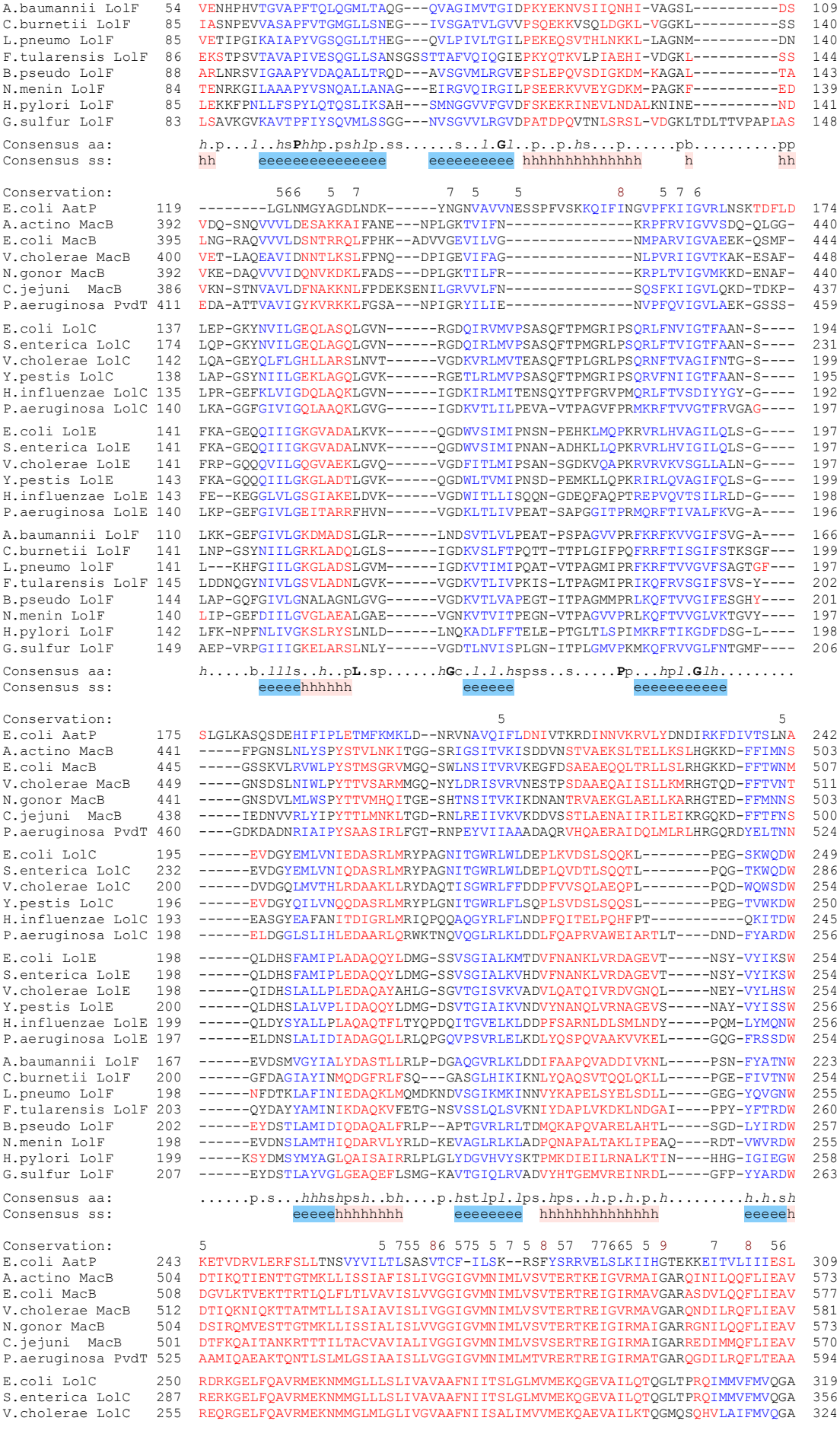
A.baumannii LolF 54 VENHPHVTGVAPFTQLQGMLTAQG---QVAGIMVTGIDPKYEKNVSIIQNHI-VAGSL---------DS 109
C.burnetii LolF 85 IASNPEVVASAPFVTGMGLLSNEG---IVSGATVLGVVPSQEKKVSQLDGKL-VGGKL---------SS 140
L.pneumo LolF 85 VETIPGIKAIAPYVGSQGLLTHEG---QVLPIVLTGILPEKEQSVTHLNKKL-LAGNM---------DN 140
F.tularensis LolF 86 EKSTPSVTAVAPIVESQGLLSANSGSSTTAFVQIQGIEPKYQTKVLPIAEHI-VDGKL---------SS 144
B.pseudo LolF 88 ARLNRSVIGAAPYVDAQALLTRQD---AVSGVMLRGVEPSLEPQVSDIGKDM-KAGAL---------TA 143
N.menin LolF 84 TENRKGILAAAPYVSNQALLANAG---EIRGVQIRGILPSEERKVVEYGDKM-PAGKF---------ED 139
H.pylori LolF 85 LEKKFPNLLFSPYLQTQSLIKSAH---SMNGGVVFGVDFSKEKRINEVLNDALKNINE---------ND 141
G.sulfur LolF 83 LSAVKGVKAVTPFIYSQVMLSSGG---NVSGVVLRGVDPATDPQVTNLSRSL-VDGKLTDLTTVPAPLAS 148
Consensus aa: h.p...l..hsPhhp.pshlp.ss.....s..l.Gl..p..p.hs...p.....pb.....pp
Consensus ss: hh eeeeeeeeeeeeee eeeeeeeee hhhhhhhhhhhhh h hh
Conservation: 566 5 7 7 5 5 8 5 7 6
E.coli AatP 119 --------LGLNMGYAGDLNDK------YNGNVAVVNESSPFVSKKQIFINGVPFKIIGVRLNSKTDFLD 174
A.actino MacB 392 VDQ-SNQVVVLDESAKKAIFANE---NPLGKTVIFN---------------KRPFRVIGVVSDQ-QLGG- 440
E.coli MacB 395 LNG-RAQVVVLDSNTRRQLFPHK--ADVVGEVILVG---------------NMPARVIGVAEEK-QSMF- 444
V.cholerae MacB 400 VET-LAQEAVIDNNTLKSLFPNQ---DPIGEVIFAG---------------NLPVRIIGVTKAK-ESAF- 448
N.gonor MacB 392 VKE-DAQVVVIDQNVKDKLFADS---DPLGKTILFR---------------KRPLTVIGVMKKD-ENAF- 440
C.jejuni MacB 386 VKN-STNVAVLDFNAKKNLFPDEKSENILGRVVLFN---------------SQSFKIIGVLQKD-TDKP- 437
P.aeruginosa PvdT 411 EDA-ATTVAVIGYKVRKKLFGSA---NPIGRYILIE---------------NVPFQVIGVLAEK-GSSS- 459
E.coli LolC 137 LEP-GKYNVILGEQLASQLGVN------RGDQIRVMVPSASQFTPMGRIPSQRLFNVIGTFAAN-S---- 194
S.enterica LolC 174 LQP-GKYNVILGEQLAGQLGVN------RGDQIRLMVPSASQFTPMGRLPSQRLFTVIGTFAAN-S---- 231
V.cholerae LolC 142 LQA-GEYQLFLGHLLARSLNVT------VGDKVRLMVTEASQFTPLGRLPSQRNFTVAGIFNTG-S---- 199
Y.pestis LolC 138 LAP-GSYNIILGEKLAGQLGVK------RGETLRLMVPSASQFTPMGRIPSQRVFNIIGTFAAN-S---- 195
H.influenzae LolC 135 LPR-GEFKLVIGDQLAQKLGVN------IGDKIRLMITENSQYTPFGRVPMQRLFTVSDIYYGY-G---- 192
P.aeruginosa LolC 140 LKA-GGFGIVIGQLAAQKLGVG------IGDKVTLILPEVA-VTPAGVFPRMKRFTVVGTFRVGAG---- 197
E.coli LolE 141 FKA-GEQQIIIGKGVADALKVK------QGDWVSIMIPNSN-PEHKLMQPKRVRLHVAGILQLS-G---- 197
S.enterica LolE 141 FKA-GEQQIIIGKGVADALNVK------QGDWVSIMIPNAN-ADHKLLQPKRVRLHVIGILQLS-G---- 197
V.cholerae LolE 141 FRP-GQQQVILGQGVAEKLGVQ------VGDFITLMIPSAN-SGDKVQAPKRVRVKVSGLLALN-G---- 197
Y.pestis LolE 143 FKA-GQQQIIILGKGLADTLGVK------QGDWLTVMIPNSD-PEMKLLQPKRIRLQVAGIFQLS-G---- 199
H.influenzae LolE 143 FE--KEGGLVLGSGIAKELDVK------VGDWITLLISQQN-GDEQFAQPTREPVQVTSILRLD-G---- 198
P.aeruginosa LolE 140 LKP-GEFGIVLGEITARRFHVN------VGDKLTLIVPEAT-SAPGGITPRMQRFTIVALFKVG-A---- 196
A.baumannii LolF 110 LKK-GEFGIVLGKDMADSLGLR------LNDSVTLVLPEAT-PSPAGVVPRFKRFKVVGIFSVG-A---- 166
C.burnetii LolF 141 LNP-GSYNIILGRKLADQLGLS------IGDKVSLFTPQTT-TTPLGIFPQFRRFTISGIFSTKSGF--- 199
L.pneumo lolF 141 L---KHFGIILGKGLADSLGVM------IGDKVTIMIPQAT-VTPAGMIPRFKRFTVVGVFSAGTGF--- 197
F.tularensis LolF 145 LDDNQGYNIVLGSVLADNLGVK------VGDKVTLIVPKIS-LTPAGMIPRIKQFRVSGIFSVS-Y---- 202
B.pseudo LolF 144 LAP-GQFGIVLGNALAGNLGVG------VGDKVTLVAPEGT-ITPAGMMPRLKQFTVVGIFESGHY---- 201
N.menin LolF 140 LIP-GEFDIILGVGLAEALGAE------VGNKVTVITPEGN-VTPAGVVPRLKQFTVVGLVKTGVY---- 197
H.pylori LolF 142 LFK-NPFNLIVGKSLRYSLNLD------LNQKADLFFTELE-PTGLTLSPIMKRFTIKGDFDSG-L---- 198
G.sulfur LolF 149 AEP-VRPGIIIGKELARSLNLY------VGDTLNVISPLGN-ITPLGMVPKMKQFRVVGLFNTGMF---- 206
Consensus aa: h.....b.llls..h..pL.sp.....hGc.l.l.hspss..s.....Pp...hpl.Glh.....
Consensus ss: eeeeehhhhhh eeeeee eeeeeeeeeee
Conservation: 5 5
E.coli AatP 175 SLGLKASQSDEHIFIPLETMFKMKLD--NRVNAVQIFLDNIVTKRDINNVKRVLYDNDIRKFDIVTSLNA 242
A.actino MacB 441 -----FPGNSLNLYSPYSTVLNKITGG-SRIGSITVKISDDVNSTVAEKSLTELLKSLHGKKD-FFIMNS 503
E.coli MacB 445 -----GSSKVLRVWLPYSTMSGRVMGQ-SWLNSITVRVKEGFDSAEAEQQLTRLLSLRHGKKD-FFTWNM 507
V.cholerae MacB 449 -----GNSDSLNIWLPYTTVSARMMGQ-NYLDRISVRVNESTPSDAAEQAIISLLKMRHGTQD-FFTVNT 511
N.gonor MacB 441 -----GNSDVLMLWSPYTTVMHQITGE-SHTNSITVKIKDNANTRVAEKGLAELLKARHGTED-FFMNNS 503
C.jejuni MacB 438 -----IEDNVVRLYIPYTTLMNKLTGD-RNLREIIVKVKDDVSSTLAENAIIRILEIKRGQKD-FFTFNS 500
P.aeruginosa PvdT 460 ----GDKDADNRIAIPYSAASIRLFGT-RNPEYVIIAAADAQRVHQAERAIDQLMLRLHRGQRDYELTNN 524
E.coli LolC 195 ------EVDGYEMLVNIEDASRLMRYPAGNITGWRLWLDEPLKVDSLSQQKL--------PEG-SKWQDW 249
S.enterica LolC 232 ------EVDGYEMLVNIQDASRLMRYPAGNITGWRLWLDEPLQVDTLSQQTL--------PQG-TKWQDW 286
V.cholerae LolC 200 ------DVDGQLMVTHLRDAAKLLRYDAQTISGWRLFFDDPFVVSQLAEQPL--------PQD-WQWSDW 254
Y.pestis LolC 196 ------EVDGYQILVNQQDASRLMRYPLGNITGWRLFLSQPLSVDSLSQQSL--------PEG-TVWKDW 250
H.influenzae LolC 193 ------EASGYEAFANITDIGRLMRIQPQQAQGYRLFLNDPFQITELPQHFPT-----------QKITDW 245
P.aeruginosa LolC 198 ------ELDGGLSLIHLEDAARLQRWKTNQVQGLRLKLDDLFQAPRVAWEIARTLT----DND-FYARDW 256
E.coli LolE 198 ------QLDHSFAMIPLADAQQYLDMG-SSVSGIALKMTDVFNANKLVRDAGEVT-----NSY-VYIKSW 254
S.enterica LolE 198 ------QLDHSFAMIPLEDAQQYLDMG-SSVSGIALKVHDVFNANKLVRDAGEVT-----NSY-VYIKSW 254
V.cholerae LolE 198 ------QIDHSLALLPLEDAQAYAHLG-SGVTGISVKVADVLQATQIVRDVGNQL-----NEY-VYLHSW 254
Y.pestis LolE 200 ------QLDHSLALVPLIDAQQYLDMG-DSVTGIAIKVNDVYNANQLVRNAGEVS-----NAY-VYISSW 256
H.influenzae LolE 199 ------QLDYSYALLPLAQAQTFLTYQPDQITGVELKLDDPFSARNLDLSMLNDY-----PQM-LYMQNW 256
P.aeruginosa LolE 197 ------ELDNSLALIDIADAGQLLRLQPGQVPSVRLELKDLYQSPQVAAKVVKEL-----GQG-FRSSDW 254
A.baumannii LolF 167 ------EVDSMVGYIALYDASTLLRLP-DGAQGVRLKLDDIFAAPQVADDIVKNL-----PSN-FYATNW 223
C.burnetii LolF 200 ------GFDAGIAYINMQDGFRLFSQ---GASGLHIKIKNLYQAQSVTQQLQKLL-----PGE-FIVTNW 254
L.pneumo LolF 198 ------NFDTKLAFINIEDAQKLMQMDKNDVSGIKMKINNVYKAPELSYELSDLL-----GEG-YQVGNW 255
F.tularensis LolF 203 ------QYDAYYAMINIKDAQKVFETG-NSVSSLQLSVKNIYDAPLVKDKLNDGAI----PPY-YFTRDW 260
B.pseudo LolF 202 ------EYDSTLAMIDIQDAQALFRLP--APTGVRLRLTDMQKAPQVARELAHTL-----SGD-LYIRDW 257
N.menin LolF 198 ------EVDNSLAMTHIQDARVLYRLD-KEVAGLRLKLADPQNAPALTAKLIPEAQ----RDT-VWVRDW 255
H.pylori LolF 199 -----KSYDMSYMYAGLQAISAIRRLPLGLYDGVHVYSKTPMKDIEILRNALKTIN----HHG-IGIEGW 258
G.sulfur LolF 207 ------EYDSTLAYVGLGEAQEFLSMG-KAVTGIQLRVADVYHTGEMVREINRDL-----GFP-YYARDW 263
Consensus aa: ......p.s...hhhshpsh..bh....p.hstlpl.lps.hps..h.p.h.p.h.........h.h.sh
Consensus ss: eeeeehhhhhhhh eeeeeeee hhhhhhhhhhhhhh eeeeeh
Conservation: 5 5 755 86 575 5 7 5 8 57 77665 5 9 7 8 56
E.coli AatP 243 KETVDRVLERFSLLTNSVYVILTLSASVTCF-ILSK--RSFYSRRVELSLKIIHGTEKKEITVLIIIESL 309
A.actino MacB 504 DTIKQTIENTTGTMKLLISSIAFISLIVGGIGVMNIMLVSVTERTKEIGVRMAIGARQINILQQFLIEAV 573
E.coli MacB 508 DGVLKTVEKTTRTLQLFLTLVAVISLVVGGIGVMNIMLVSVTERTREIGIRMAVGARASDVLQQFLIEAV 577
V.cholerae MacB 512 DTIQKNIQKTTATMTLLISAIAVISLIVGGIGVMNIMLVSVTERTREIGVRMAVGARQNDILRQFLIEAV 581
N.gonor MacB 504 DSIRQMVESTTGTMKLLISSIALISLVVGGIGVMNIMLVSVTERTKEIGIRMAIGARRGNILQQFLIEAV 573
C.jejuni MacB 501 DTFKQAITANKRTTTILTACVAVIALIVGGIGVMNIMLVSVSERTREIGIRMAIGARREDIMMQFLIEAV 570
P.aeruginosa PvdT 525 AAMIQAEAKTQNTLSLMLGSIAAISLLVGGIGVMNIMLMTVRERTREIGIRMATGARQGDILRQFLTEAA 594
E.coli LolC 250 RDRKGELFQAVRMEKNMMGLLLSLIVAVAAFNIITSLGLMVMEKQGEVAILQTQGLTPRQIMMVFMVQGA 319
S.enterica LolC 287 RERKGELFQAVRMEKNMMGLLLSLIVAVAAFNIITSLGLMVMEKQGEVAILQTQGLTPRQIMMVFMVQGA 356
V.cholerae LolC 255 REQRGELFQAVRMEKNMMGLMLGLIVGVAAFNIISALIMVVMEKQAEVAILKTQGMQSQHVLAIFMVQGA 324

```
Y.pestis LolC      251  RDRKGELFQAVRMEKNMMGLLLSLIIAVAAFNIITSLGLLVMEKQGEVAILQTQGLSRRQIMLVFMVQGA  320
H.influenzae LolC 246  RVQKGEFFQAVRMEKNMMGLLISLIIVVAISNIVTSLSLMVVDKQGEIAILQTQGLTKSQVRSVFIYQGL  315
P.aeruginosa LolC 257  TRSHGNLYQAIRMEKTMIGLLLLLIVAVAAFNIISTLVMVVTDKKSDIAILRTLGATPGQIMATFMVQGT  326

E.coli LolE        255  IGTYGYMYRDIQMIRAIMYLAMVLVIGVACFNIVSTLVMAVKDKSGDIAVLRTLGAKDGLIRAIFVWYGL  324
S.enterica LolE    255  IGTYGYMYRDIQMIRAIMYLAMILVIGVACFNIVSTLVMAVKDKSGDIAVLRTLGAKDGLIRAIFVWYGL  324
V.cholerae LolE    255  QQKYGFLYRDIQLVRTIMYLVMVLVIGVASFNIVSTLMMAVKDRAGEIAILRTMGATDGLIKRIFVWQGV  324
Y.pestis LolE      257  IGTYGYMYRDIQMIRTIMYLAMVLVIGVASFNIVSTLVMAVKDKSSDIAVLRTLGAKDGLIRAIFIWYGL  326
H.influenzae LolE  257  ISKFGYMYRDIQLIRTVMYIAMVLVIGVACFNIVSTLIMAVKDKQGDIAIMRTLGANNAFIKRIFIWYGL  326
P.aeruginosa LolE  255  TRTQGSLFNAMKMEKTMIGLLLLLIIAVAAFNIIATLIMVVADKRTDIAILRTLGATPRQIMAIFMVQGT  324

A.baumannii LolF   224  TYTHGNLFNAIQMEKTLVGLLLVLIIVVAAFNIVSSLVMVVTDKKSDIAILRTLGASPSMITKIFMVQGT  293
C.burnetii LolF    255  TEQFGSFFKAIAMEKTIMFVILLLIVGVAIFNLVSTLVMVVNDKRADIAILRTLGASPRTIMSIFVIQGA  324
L.pneumo LolF      256  TQQFGAFFEAVKMEKTMMFMILLLIIAVAAFNLVSSLVMVVNDKQAEIAILRTIGATPSTILWVFIVQGM  325
F.tularensis LolF  261  TDENKSFFDALKMEKTMMFFILLLIITVAVFNLLSSLVMVVTDKRSDIAILRTMGMSSRQIITVFIYQGF  330
B.pseudo LolF      258  TQQNKTWFSAVQIEKRMMFIILTLIIAVAAFNLVSSLVMTVTNKQADIAILRTLGAQPGSIMKIFVVQGV  327
N.menin LolF       256  TFSNRSYFEAVELEKRMMFIILTLIIAVAAFNLVSSLVMAVTEKQADIAILRTLGLSPGGVMKIFMVQGA  325
H.pylori LolF      259  WQQNGNFFSAMELEKRALFIVLMLIILMASLNIISSLLMVVMNRRKEIALLFSMGSSQKEIQKTFFYLGN  328
G.sulfur LolF      264  MQMNKNILFALKTEKMVMFIILTLIVLVAAFGIASTLFMVVMEKTKDIAILKSMGATGRSIMKIFVLEGL  333

Consensus aa:           ......hhpshphbp.hh.hlhhl.l.Vtthslhs.hhhsV.-+p.-ltl..hhGhp...I...Fhhpth
Consensus ss:           hhhhhhhhhhhhhhhhhhhhhhhhhhhhhhhhhhhhhhhhhhhhhhhhhhhhhhh    hhhhhhhhhhhh

Conservation:             5  8   8  56             5                5   5              7  5   5
E.coli AatP        310  IMLSVCLFISII-------HAGVIMHIIKYFLDVKIS------IRTTMITISLAYVLLVFISA---NIIF  363
A.actino MacB      574  LICLIGGVAGILLSVLIGVLFNSFIT-------------------DFSMDFSTASIVTAVLFSTLIGVLF  594
E.coli MacB        578  LVCLVGGALGITLSLLIAFTLQLFLP-------------------GWEIGFSPLALLLAFLCSTVTGILF  628
V.cholerae MacB    582  LVCLCGGAIGIGVAYLIGGLFATLGS-------------------SFSMIYSTTSIISAFLCSTLIGVLF  632
N.gonor MacB       574  LICIIGGLVGVGLSAAVSLVFNHFVT-------------------DFPMDISAASVIGAVACSTGIGIAF  624
C.jejuni  MacB     571  MICTIGAILGVILSIFVIFAFNTLST-------------------DFPMILNAYSVLLGLLSSMFIGVVF  621
P.aeruginosa PvdT  595  MLSVVGGLAGIALALCIGGVLLLGQ--------------------VAVAFSLSAIVGAFSCALVTGLVF  643

E.coli LolC        320  SAGIIGAILGAALGALLASQLNNLMPIIGVLL----------DGAALPVAIEPLQVIVIALVAMAIALLS  379
S.enterica LolC    357  SAGIIGALLGAALGALLASQLNNLMPIIGAFL----------DGAALPVAIEPLQVIVIALVAMAIALLS  416
V.cholerae LolC    325  SSGVIGALVGGLLGVLLAANLNSLMEALGVALFS--------VGGSLPVAIDPLQIVLVIVLAIVLSLLA  386
Y.pestis LolC      321  TAGVIGALLGAGLGVLLASQLNTLIPILGVLI----------DGATLPVEIDPLQVTVIALLAMVIALLS  380
H.influenzae LolC  316  LVGFVGTLLGAILGVLATLNLTDIVSAVNP------------QGVFLPTELSFVQMIFVIGFSLLLSLLS  373
P.aeruginosa LolC  327  VIGVIGTLVGGVLGVVAALNVSAWISALEKLLGHQFLASDVYFIDYLPSQLMLDDVVLVCGAALVLSFFA  396

E.coli LolE        325  LAGLFGSLCGVIIGVVVSLQLTPIIEWIEKLIGHQFLSSDIYFIDFLPSELHWLDVFYVLVTALLLS-LA  393
S.enterica LolE    325  LAGLLGSLIGVAIGVVVSLQLTAIINGIEKAIGHQFLSGDIYFIDFLPSELHWLDVVYVLVTALLLSLLA  394
V.cholerae LolE    325  FSGVLGSVVGSVLGMVVAFNLTPLIKGLEHLIGHQFLSGDIYFVDFLPSQVEWADVVLVSGTAIVLSLLA  394
Y.pestis LolE      327  LAGLIGSISGAVIGVIVSLQLTTIIRGLEKMVGHQFLSSDIYFIDFLPSELRWFDVACVLATALVLSLIA  396
H.influenzae LolE  327  QAGMKGCLIGIVLGIILALNLTTFIQGIEWVIGKKLLSGDVYFVDFLPSELHWLDVLMVLVAALALSLMA  396
P.aeruginosa LolE  325  VIGVIGTVIGGVLGVFAALNITGMIDRIERLVGHKVFSSDVYFINYLPSDLQVLDVVLICSAALLMSFLA  394

A.baumannii LolF   294  VIGVIGTVAGTVLGVILALTISDIISWFNNVLGLNLF--DAYFVHYLPSYLRWQDVTIIVIVSLLLSFLA  361
C.burnetii LolF    325  IVGIVGTLIGVIGGVILAVNATAIVNGIQQIFHVQFLKSSIYFVNFLPSRLQWLDVLNVSLIAFALSLIA  394
L.pneumo LolF      326  MVGLVGTILGLLGGLVLANNATEIVNALQSFFQVKVLSSSIYFVDYLPSKIMFRDLWQVCAMALLMSFAA  395
F.tularensis LolF  331  IIGLIGTVIGVLLGILLSTYATEIVNFIQNLTGKQFLSASVYLINYIPSELMWSDVIKVTLVSMFLSFLA  400
B.pseudo LolF      328  TIGFVGTATGVALGCLIAWSIPWLIPMIEHAFGVQFLPPSVYFISELPSELVAGDVIKIGVIAFALSALA  397
N.menin LolF       326  FSGFFGTLAGVVCGVLLGWNVGRVVAFFENLLGVHLINSQVYFIDYLPSDVDMGDVALIACISLGLSFVA  395
H.pylori LolF      329  IIGLGGVA----LGVVLAF----LSMYLLSVFPIISLPADVYGINTLPLNLSLMDFTLTLIGSVIIVGLS  390
G.sulfur LolF      334  IIGISGTAIGVIGGLLVALNLEPIVGVIQRVTGFELFSKDVYYLDHFPSQVVPSDVLLISVTAVIISLVA  403

Consensus aa:           hhthhGshhGhhlthlltl..hs.h...l..............s.hs..lph.plh.hhh.thhlthlh
Consensus ss:           hhhhhhhhhhhhhhhhhhhhhhhhhhhhhhh                ee hhhhhhhhhhhhhhhh

Conservation:             5 597  76   75 68
E.coli AatP        364  G----RLFFSINPVNAIKGKIE  381
A.actino MacB      594  GYMPAKKAAELNPITALAQE--  644
E.coli MacB        629  GWLPARNAARLDPVDALARE--  648
V.cholerae. MacB   633  GYLPAKNAAQLNPIDALARE--  652
N.gonor MacB       625  GFMPANKAAKLNPIDALAQD--  644
C.jejuni  MacB     622  GFFPARNAANLNPISALSKE--  641
P.aeruginosa PvdT  644  GFMPARKAAQLDPVAALASQ--  663

E.coli LolC        380  TLYPSWRAAATQPAEALRYE--  399
S.enterica LolC    417  TLYPSWRAAATQPAEALRYE--  436
V.cholerae LolC    387  TLFPAYRASSVQPAEALRYE--  406
Y.pestis LolC      381  TLYPSWRAAAAQPAEALRYE--  400
H.influenzae LolC  374  TLYPAYRAAKVEPAAALRYE--  393
P.aeruginosa LolC  397  TLYPAWRAARTQPAEALRYE--  416

E.coli LolE        394  SWYPARRASNIDPARVLSGQ--  413
S.enterica LolE    395  SWYPARRASNIDPARVLSGQ--  414
V.cholerae LolE    395  TWYPARRASRLNPAQVLSSK--  414
Y.pestis LolE      397  SWYPARRASRIDPARVLSGQ--  416
H.influenzae LolE  397  SLYPASRAAKLQPAQVLSSH--  416
P.aeruginosa LolE  395  TLYPSWRAARTQPAESLRYE--  414

A.baumannii LolF   362  TIYPALRAAKVQPAEALRYE--  381
C.burnetii LolF    395  TIYPAFIAFRTEPAEALRYE--  414
L.pneumo LolF      396  TIYPAWRASKTVIAEALHYE--  415
F.tularensis LolF  401  TLYPAWSASKVQPVEALRYE--  420
B.pseudo LolF      398  TLYPSWRGAKVRPAEALRYE--  417
N.menin LolF       396  TLYPSRRASKTQPAEALRYE--  415
H.pylori LolF      391  SYYPSKKASTIDALSVLRNE--  410
G.sulfur LolF      404  TLYPSWQASRLPPAEALRYE--  423

Consensus aa:           shhPt.pAtphpPhphL..c..
Consensus ss:           hhhhhhhhh   hhhhh
```

Figure S4. Protein alignment of members of the MacB superfamily. Sequence alignment was generated with Promals3D excluding the nucleotide-binding domain of MacB and PvdT. Sequences corresponding to predicted helices are highlighted in *red*, β-sheets in *blue.* Abbreviations are as follows E.coli, *Escherichia coli*; A.actino, Aggregatibacter actinomycetemcomitans; V.cholerae, *Vibrio cholerae*; N.gonor, *Neisseria gonorrhoeae* ; C.jejuni, *Campylobacter jejuni*; P.aeruginosa, *Pseudomonas aeruginosa*; S.enterica, *Salmonella enterica* serovar Typhimurium; Y.pestis, *Yersinia pestis*; H.influenzae, *Haemophilus influenzae*; A.baumannii, *Acinetobacter baumannii*; C.burnetii, *Coxiella burnetii*; L.pneumo, *Legionella pneumophila*; F.tularensis, *Francisella tularensis*; B.pseudo, *Burkholderia pseudomallei*; N.menin, *Neisseria meningitidis*; H.pylori, *Helicobacter pylori*; G.sulfur, *Geobacter sulfurreducens*.

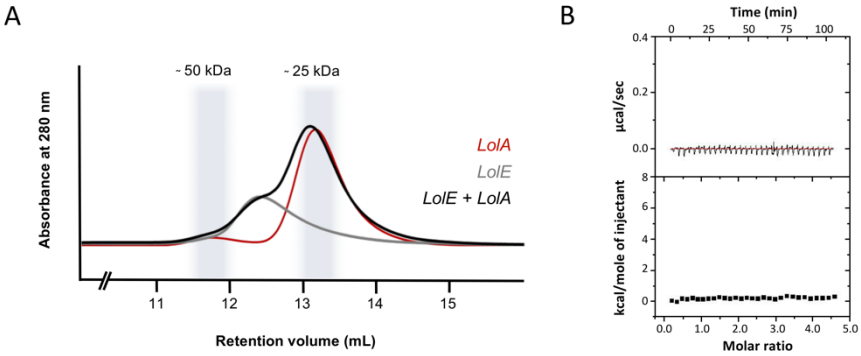

Figure S5. LolA does not bind to the LolE periplasmic domain. (A) Size-exclusion chromatography profiles for LolA, LolE periplasmic domain and a mixture of the two proteins. (B) Isothermal titration calorimetry using LolE and LolA. Both experiments were performed under conditions where LolC and LolA interact with high affinity.

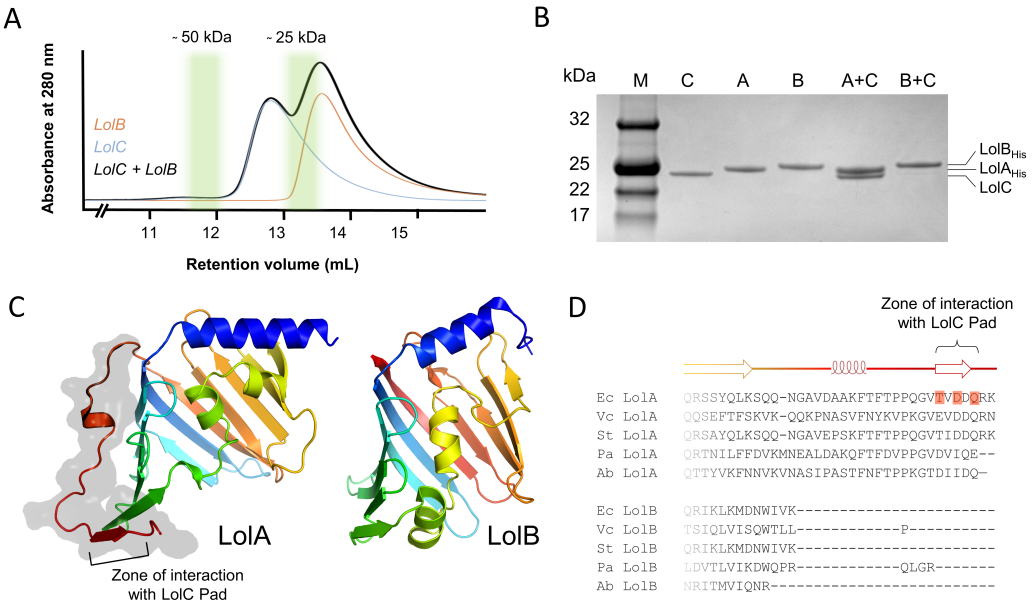

Figure S6. LolB does not interact with LolC. (A) Size-exclusion chromatography experiment for LolB, LolC periplasmic domain and a mixture of the two proteins. (B) Assessment of the *in vitro* interaction of LolC with LolA or LolB. Untagged LolC periplasmic domain was added to His-tagged LolA (A+C) or LolB (B+C) immobilized on IMAC resin. After washing, bound proteins were eluted with imidazole and analysed on SDS-PAGE. Purified LolC periplasmic domain, C; LolA, A; and LolB, B are loaded as a reference. Molecular weights of protein standards (M) are indicated. (C) Comparison of LolA (6F3Z) and LolB (1IWM) showing the presence of an extra loop in LolA (dark surface). (D) Sequence alignment of LolA and LolB proteins showing the C-terminal region. Secondary structural elements of LolA are indicated above the sequence alignment. Residues in *E. coli* LolA that interact with the LolC Pad are highlighted in *red*. Abbreviations are as follows Ec, *Escherichia coli*; Vc, *Vibrio cholerae*; St, *Salmonella enterica* serovar Typhi; Pa, *Pseudomonas aeruginosa*; Ab, *Acinetobacter baumannii*.

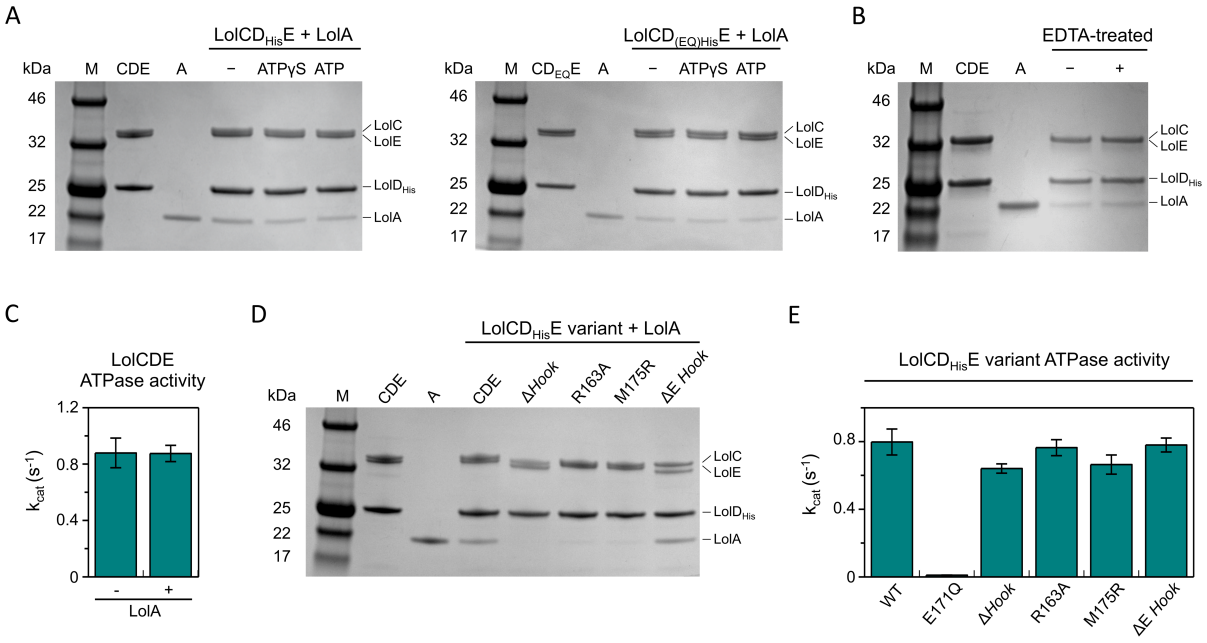

Figure S7. LolA-binding and ATPase assays for wild-type and variant LolCDE complexes. (A) *In vitro* interaction of LolA with wild-type LolCDE (*left*) or LolCD(E171Q)E variant (*right*) in the presence and absence of ATP or ATPγS. Wild-type LolCDE or E171Q variant bearing a His-tag on LolD were incubated with no nucleotide (-), 1 mM ATP or ATPγS as indicated, and immobilized on IMAC resin. Untagged LolA was then added, the resin washed, and bound proteins eluted with imidazole and analysed on SDS-PAGE. Purified proteins loaded as references are LolCDE, CDE; and LolA, A. Molecular weights of protein standards (M) are indicated. (B) *In vitro* interaction of LolA with wild-type LolCDE untreated or treated with 5 mM EDTA. (C) ATPase assays for wild-type LolCDE in the absence and presence of 5 μM LolA. Results correspond to the mean ± standard deviation for triplicate determinations. (D) Assessment of the *in vitro* interaction of LolA with wild-type or variant LolCDE. LolA binding assay in the absence of nucleotide for wild-type LolCDE and indicated variants: ΔHook, R163A, M175R, correspond to mutations in LolC component of LolCDE; ΔE Hook corresponds to LolCDE with the Hook removed from LolE. (E) ATPase assays for wild-type and variant LolCDE complexes. Results correspond to the mean ± standard deviation for triplicate determinations.

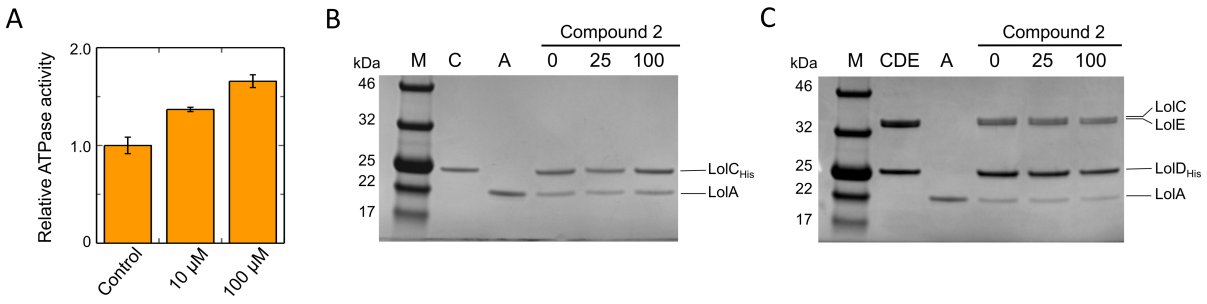

Figure S8. LolCDE inhibitor Compound 2 stimulates ATPase activity but does not interfere with LolA binding. (A) ATPase assay for wild-type LolCDE in the presence of 0, 10 or 100 μM Compound 2. ATP hydrolysis rates correspond to the mean ± standard deviation for triplicate determinations. (B) Effect of Compound 2 on the *in vitro* interaction of LolC and LolA. His-tagged LolC periplasmic domain was incubated with the indicated concentration (μM) of Compound 2 and immobilized on IMAC resin prior to the addition of untagged LolA. After washing, bound proteins were eluted with imidazole and analysed on SDS-PAGE. Purified LolC periplasmic domain, C; and LolA, A are loaded as a reference. Molecular weights of protein standards (M) are indicated. (C) Effect of Compound 2 on the *in vitro* interaction of His-tagged LolCDE and LolA.

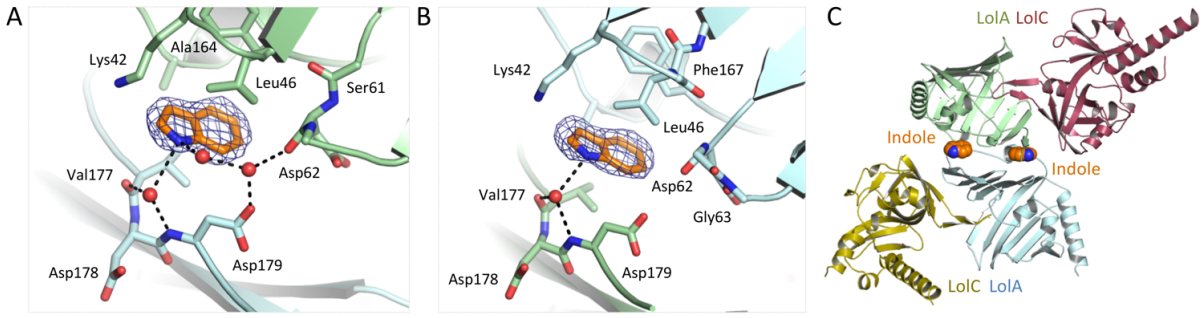

Figure S9. Additional electron density in the LolA·LolC structure suggestive of indole. (A, B) Sites within the asymmetric unit with additional difference map electron density suggestive of indole. The difference electron density map is shown as a *blue* mesh contoured at 3 σ. (C) Locations of putative indole sites within the context of the asymmetric unit. The presence of indole was biochemically confirmed for the *E. coli* culture used to express these proteins, but not for the protein solution. We therefore chose to omit indole from the deposited coordinates while highlighting its possible presence here.

Supplemental Tables

Table S1. X-ray data and refinement statistics

	LolA bound to LolC periplasmic domain	LolC ΔHook	LolA F47E
PDB code	6F3Z	6F49	6FHM
Data Collection			
Beamline	ESRF 30B	ESRF 30B	Diamond I03
Wavelength (Å)	0.9763	0.9763	0.9763
Crystal Parameters			
Space Group	$P2_1\ 2_1\ 2$	$P2_1\ 2_1\ 2_1$	$P2\ 2_1\ 2_1$
Unit Cell Dimensions (Å)	146.0, 68.2, 94.8	75.3, 108.5, 109.5	61.0, 77.6, 103.6
Unit Cell Angles (°)	90, 90, 90	90, 90, 90	90, 90, 90
Mosaic Spread (°)	0.58	0.58	0.44
Reflection Data			
Resolution Range (Å)	73.01-2.00 (2.05-2.00)	62.04-2.02 (2.07-2.02)	62.11-2.39 (2.48-2.39)
Unique Reflections	61745 (4379)	58914 (4321)	20165 (2087)
R_{sym}	0.103 (0.844)	0.166 (0.684)	0.196 (1.167)
I/σ(I)	10.6 (2.2)	6.7 (2.0)	6.7 (2.1)
CC½	0.997 (0.883)	0.990 (0.704)	0.984 (0.893)
Completeness (%)	95.8 (97.0)	99.1 (99.5)	100.0 (100.0)
Multiplicity	10.2 (9.9)	5.0 (5.2)	11.4 (11.8)
Wilson B ($Å^2$)	33.5	14.1	47.2
Refinement			
Resolution (Å)	73.01 (2.00)	62.04 (2.02)	62.11 (2.39)
Number of Reflections	58544	55872	19110
R_{work}	0.2022	0.1884	0.2147
R_{free}	0.2492	0.2328	0.2693
Rms (Bond Lengths) (Å)	0.019	0.015	0.015
Rms (Bond Angles) (°)	1.85	1.70	1.67
Model Composition			
Protein atoms	6536	6639	2987
Waters	152	452	48
Other	0	84	18
Model B-factors			
Protein atoms ($Å^2$)	47.1	22.9	61.4
Waters ($Å^2$)	42.6	26.9	54.1
Other	-	39.1	68.6
Ramachandran Statistics			
Favoured (%)	97.0	99.0	95.5
Allowed (%)	3.0	1.0	4.5
Outliers (%)	0.0	0.0	0.0

Values in parentheses indicate the outer resolution bin.
Reflection data is as reported by Aimless (52).
Refinement statistics as reported by Refmac (55).
Ramachandran statistics from Rampage (56).

Table S2. ITC data for LolA binding by LolC periplasmic domain variants

	K_d (μM)	*N*	*ΔG*	*ΔH*	*-TΔS*
LolC	0.3, 0.4, 0.4, 0.5 **0.4 ± 0.1**	1.02, 0.92, 0.91, 1.21 **1.01 ± 0.14**	-8.9, -8.7, -8.7, -8.6 **-8.7 ± 0.1**	7.0, 7.7, 8.3, 6.2 **7.3 ± 0.9**	-15.9, -16.4, -17.0, -14.8 **-16.0 ± 0.9**
LolC ΔHook	No binding	-	-	-	-
LolC R163A	No binding	-	-	-	-
LolC Q171A	0.4, 0.5 **0.4 ± 0.1**	0.97, 0.99 **0.98 ± 0.01**	-8.7, -8.6 **-8.7 ± 0.1**	7.1, 7.0 **7.0 ± 0.1**	-15.8, -15.6 **-15.7 ± 0.1**
LolC F172A	4.0, 3.6 **3.8 ± 0.3**	1.02, 1.04 **1.03 ± 0.01**	-7.4, -7.4 **-7.4 ± 0.0**	8.5, 7.6 **8.0 ± 0.6**	-15.8, -15.0 **-15.4 ± 0.6**
LolC T173A	62.5, 74.3, 71.9 **69.6 ± 6**	**1.00 ***	-5.7, -5.6, -5.6 **-5.7 ± 0.1**	8.5, 8.0, 6.4 **7.6 ± 1.1**	-14.2, -13.6, -12.1 **-13.3 ±1.1**
LolC M175A	4.9, 4.0 **4.5 ± 0.6**	1.03, 1.03 **1.03 ± 0.00**	-7.2, -7.4 **-7.3 ± 0.1**	11.9, 9.8 **10.8 ± 1.5**	-19.2, -17.1 **-18.1 ± 1.4**
LolC R177A	2.5, 1.7 **2.1 ± 0.5**	0.87, 0.92 **0.90 ± 0.04**	-7.6, -7.8 **-7.7 ± 0.2**	-7.2, -7.4 **7.3 ±0.1**	-15.4, -14.8 **-15.1 ± 0.4**
LolC I178A	12.7, 10.0 **11.4 ± 1.9**	0.93, 1.11 **1.02 ± 0.13**	-6.7, -6.8 **-6.7 ± 0.1**	6.1, 6.1 **6.1 ± 0.0**	-12.8, -12.9 **-12.9 ± 0.1**
LolC Q181A	1.6, 1.4 **1.5 ± 0.1**	1.06, 1.09 **1.07 ± 0.02**	-7.9, -8.0 **7.1 ± 0.0**	7.3, 6.9 **7.1 ± 0.3**	15.2, -14.9 **-15.1 ± 0.3**
LolC R182A	26.3, 36.2 **31.2 ± 7.0**	**1.00 ***	-6.2, -6.1 **3.6 ± 0.1**	3.4, 3.8 **3.6 ± 0.3**	-9.7, -9.9 **-9.8 ± 0.1**
LolC F172R	8.4, 3.7 **6.1 ± 3.3**	1.07, 1.08 **1.08 ± 0.01**	-6.9, -7.4 **6.8 ± 0.3**	7.7, 5.8 **6.8 ± 1.4**	14.7, -13.2 **-13.9 ± 1.0**
LolC M175R	No binding	-	-	-	-

Mean ± standard deviation in bold. *ΔG*, *ΔH* and *TΔS* reported in kcal mol^{-1}. *T*=25 °C.
* Stoichiometry was fixed at 1:1 for LolA binding by the T173A and R182A LolC variants.
Fits and thermograms in **Figure S2**.

Table S3. Correlation between *in vivo* crosslinking data and the LolA·LolC crystal structure.

Photo-crosslinker substitution in LolA	Crosslink to LolC?	Nearest LolC* residue	Distance (Å)
F20		P174	6.50
V24	+	**F172**	**4.06**
Q33	+	**F172**	**2.65**
W40		P174	9.70
R43			-
D55	+	**R213**	**4.82**
L59	+	**T173**	**3.60**
K64		M175	9.26
F72	+	**R210**	**3.11**
S99			-
V114			-
K118			-
F127			-
R133			-
E144	+	**F172**	**5.19**
R149		F172	7.57
K155			-
A165			-
Q173		R182	9.72
T176	+	**R182**	**3.23**
Q180		Q181	3.01

*Nearest neighbour located more than 10 Å away are not reported.
Distance measurements are for chains A and B in the LolA·LolC crystal structure (6F3Z).
Columns 1 and 2 from Tokuda (27), columns 3 and 4 this work.

Table S4. List of primers for PCR amplification.

Primers	Description	Sequence (5' to 3')
P1	LolA_NheI_F	GCGCGCTAGCATGGATGCCGCAAGCGATCTGAAAAGC
P2	LolA_BamHI_R	GCGCGGATCCTTACTACTTACGTTGATCATCTACCGTGACGCC
P3	Soluble LolB_NdeI_F	GCGCCATATGTCCGTTACCACGCCCAAAGGTCCTG
P4	Soluble LolB_BamHI_R	GCGCGGATCCTTATTTCACTATCCAGTTATCCATTTTTAAC
P5	periLolC_NdeI_F	GCGCCATATGAACGGCTTTGAGCGCGAGCTG
P6	periLolC_BamHI_R	GCGCGGATCCTTACATATTTTTTTCCATGCGTACGGCCTG
P7	periLolC ΔHook_R	GAACAGGCGCTGGCTCGCACCTACCATCACGCGGATTTGATC
P8	periLolC_NotI_R	GCGCGCGGCCGCCATATTTTTTTCCATGCGTACGGCCTG
P9	periLolC ΔHook_F	GATCAAATCCGCGTGATGGTAGGTGCGAGCCAGCGCCTGTTC
P10	periLolE_NdeI_F	GCGCCATATGCATGGTGAAATCGAGGCG
P11	periLolE_XhoI_R	GCGCCTCGAGCCAGCTTTTAATATAAACATAGCTGTTGGTCAC
P12	periLolE ΔHook_R	GCAAACGCACACGTTTCGCACCGATCATAATCGACACCC
P13	periLolE ΔHook_F	GGGTGTCGATTATGATCGGTGCGAAACGTGTGCGTTTGC
P14	periLolC_F_BspHI	GCGCTCATGAAATACCTGCTGCCGACCGCTGC
P15	T7_F	TAATACGACTCACTATAGGG
P16	His-tag_R_HindIII	GCGCAAGCTTTTAGTGGTGGTGGTGGTGGTGCTCG
P17	LolCD_PciI_F	GCGCACATGTACCAACCTGTCGCTCTATTTATTGGCCTGCGTTACATG
P18	LolCD_NotI_R	GCGCGCGGCCGCTTAGTGGTGGTGGTGGTGGTGAGAACCCTCCGCCC CCATCAGGCTCAGTTCCGC
P19	LolE_NdeI_F	GCGCCATATGGCGATGCCTTTATCGTTATTAATTGGCCTG
P20	LolE_AvrII_R	GCGCCCTAGGTTACTGGCCGCTAAGGACTCGCGCAGG
P21	LolA F74E_F	GTTGTGTCATATGCCAGTTCTCTAAGTTTGGACGTTTCACCCACAG
P22	LolA F74E_R	CTGTGGGTGAAACGTCCAAACTTAGAGAACTGGCATATGACACAAC
P23	periLolC R163A_F	CGTTAATCGCGGTGATCAAATCGCGGTGATGGTACCATCTGCC
P24	periLolC R163A_R	GGCAGATGGTACCATCACCGCGATTTGATCACCGCGATTAACG
P25	periLolC Q171A_F	CGTGATGGTACCATCTGCCAGCGCGTTCACGCCGATGGGGCG
P26	periLolC Q171A_R	CGCCCCATCGGCGTGAACGCGCTGGCAGATGGTACCATCACG
P27	periLolC F172A_F	GGTACCATCTGCCAGCCAGGCGACGCCGATGGGGCGTATTCC
P28	periLolC F172A_R	GGAATACGCCCCATCGGCGTCGCCTGGCTGGCAGATGGTACC
P29	periLolC F172R_F	GGTACCATCTGCCAGCCAGCGCACGCCGATGGGGCGTATTCC
P30	periLolC F172R_R	GGAATACGCCCCATCGGCGTGCGCTGGCTGGCAGATGGTACC
P31	periLolC T173A_F	CCATCTGCCAGCCAGTTCGCGCCGATGGGGCGTATTCC
P32	periLolC T173A_R	GGAATACGCCCCATCGGCGCGAACTGGCTGGCAGATGG
P33	periLolC M175A_F	GCCAGCCAGTTCACGCCGGCGGGGCGTATTCCAAGCCAGC
P34	periLolC M175A_R	GCTGGCTTGGAATACGCCCCGCCGGCGTGAACTGGCTGGC
P35	periLolC M175R_F	GCCAGCCAGTTCACGCCGCGCGGGCGTATTCCAAGCCAGC
P36	periLolC M175R_R	GCTGGCTTGGAATACGCCCGCGCGGCGTGAACTGGCTGGC
P37	periLolC R177A_F	GCCAGTTCACGCCGATGGGGGCGATTCCAAGCCAGCGCCTG
P38	periLolC R177A_R	CAGGCGCTGGCTTGGAATCGCCCCCATCGGCGTGAACTGGC
P39	periLolC I178A_F	GTTCACGCCGATGGGGCGTGCGCCAAGCCAGCGCCTGTTC
P40	periLolC I178A_R	GAACAGGCGCTGGCTTGGCGCACGCCCCATCGGCGTGAAC
P41	periLolC Q181A_F	CGATGGGGCGTATTCCAAGCGCGCGCCTGTTCAATGTGATTGG
P42	periLolC Q181A_R	CCAATCACATTGAACAGGCGCGCGCTTGGAATACGCCCCATCG
P43	periLolC R182A_F	GGGCGTATTCCAAGCCAGGCGCTGTTCAATGTGATTGGC
P44	periLolC R182A_R	GCCAATCACATTGAACAGCGCCTGGCTTGGAATACGCCC
P45	LolD E171Q_F	CCTGGTACTGGCGGATCAGCCTACCGGTAACC
P46	LolD E171Q_R	GGTTACCGGTAGGCTGATCCGCCAGTACCAGG

Table S5. List of plasmid constructs used in this study.

Name	Description	Reference
pET28a	Expression vector	Novagen
pET24a	Expression vector	Novagen
pET26b	Vector encoding pelB signal sequence	Novagen
pETDuet-1	Expression vector	Novagen
pET28-LolA	Expresses LolA (residues 22-203) with an N-terminal His-tag	This study
pET24-LolA	Expresses LolA (residues 22-203) with a C-terminal His-tag	This study
pET28-mLolB	Expresses mLolB (residues 23-207) with an N-terminal His-tag	This study
pET28-LolA(F47E)	Expresses LolA F47E (residues 22-203) with an N-terminal His-tag	This study
pET24-periLolC	Expresses LolC (residues 48-266) with a C-terminal His-tag	(33)
pET28-periLolC	Expresses LolC (residues 48-266) with an N-terminal His-tag	This study
pET24-periLolC(ΔHook)	Expresses LolC (residues 48-266) with a C-terminal His-tag. Residues 167-179 replaced by a GA linker	This study
pET24-periLolC(XnY)	Expresses LolC (residues 48-266) with a C-terminal His-tag, residue X at position n mutated to residue Y	This study
pET24-periLolE	Expresses LolE (residues 65-254) with a C-terminal His-tag	This study
pET24-periLolE(ΔHook)	Expresses LolE (residues 65-254) with a C-terminal His-tag. Residues 171-182 replaced by a GA linker	This study
pETDuet-LolCDE	*lolCD* cloned in the first MCS of pETDuet-1 with a C-terminal His-tag on *lolD, lolE* cloned in the 2nd MCS	This study
pETDuet-LolC(R163A)DE	Expresses LolCDE with an R163A variant of LolC	This study
pETDuet-LolC(M175R)DE	Expresses LolCDE with an M175R variant of LolC	This study
pETDuet-LolCD(E171Q)E	Expresses LolCDE with an E171Q variant of LolD	This study
pETDuet-LolC(ΔHook)DE	Expresses LolCDE with residues 167-179 of LolC replaced by a GA linker	This study
pETDuet-LolCDE(ΔHook)	Expresses LolCDE with residues 171-182 of LolE replaced by a GA linker	This study
pBAD18-pelBperiLolC	Expresses LolC (residues 48-266) with an N-terminal PelB signal peptide and a C-terminal His-tag	This study
pBAD18-pelBperiLolC(ΔHook)	Expresses LolC (residues 48-266) with an N-terminal PelB signal peptide and a C-terminal His-tag. Residues 167-179 replaced by a GA linker	This study
pBAD18-pelBperiLolC(XnY)	Expresses LolC (residues 48-266) with an N-terminal PelB signal peptide and a C-terminal His-tag. Residue X at position n mutated to residue Y	This study

Supplemental Movies

Movie 1. Roving camera tour of the LolA·LolC structure showing representative electron density. A weighted $2|F_o|-|F_c|$ electron density map, calculated with model phases, is shown as *blue* mesh contoured at 1 σ.

Movie 2. Molecular morph showing conformational changes in LolA due to LolC binding. *Left*, cartoon structure of LolA alternating between its conformation in isolation (1IWL) and within the LolA·LolC complex (6F3Z). *Right*, the same morph using a surface representation of LolA (*yellow*) with the LolC Hook (*teal*). Orientations differ by a quarter turn about the horizontal axis; on the left hand side, the mouth of LolA is located at the bottom of the frame, on the right hand side, it is viewed face-on.

Movie 3. Electron density for the LolA F47E variant. One monomer is coloured in *red*, one in *blue* to demonstrate the strand exchange between the two monomers, within the domain-swapped dimer. The glutamate residues at position 47 are shown in *yellow*. A weighted $2|F_o|-|F_c|$ electron density map, calculated with model phases, is shown as *blue* mesh contoured at 1 σ.

Supplemental Methods

Construction of strains and plasmids

Details of the primer sequences and constructs used in this study appear in **Tables S4** and **S5** respectively. For cytoplasmic expression of LolA, the mature domain of LolA (residues 22-203) lacking the N-terminal secretion signal was amplified from *E. coli* M1655 genomic DNA using primers P1/P2, digested NheI-BamHI, and inserted into pET28a (Novagen) digested with the same enzymes. The resultant vector, pET28-LolA, encodes N-terminal His-tagged mature LolA. Similarly, a plasmid expressing the mature domain of LolB (residues 23-207) with an N-terminal His-tag was amplified with primers P3/P4, digested NdeI-BamHI and ligated into pET28a resulting in pET28-mLolB. pET28-periLolC encoding LolC periplasmic domain (residues 48-266) with an N-terminal thrombin-cleavable His-tag was created by amplification with P5/P6, digestion with NdeI/BamHI and ligation into pET28a digested with the same enzymes. pET24-periLolC encoding the C-terminally His-tagged periplasmic domain of LolC was previously described (33). Residues 167-179 inclusive were replaced by a Gly-Ala linker by two-step PCR using primers P5/P7 and P8/P9. A mixture of these reactions served as a template for a final reaction with P5/P8. Digestion of this product with NdeI-NotI and introduction into NdeI-NotI digested pET24a resulted in pET24-periLolC(ΔHook). The extent of the periplasmic region of LolE (residues 65-254) was determined using the periLolC structure (5NAA) as a guide and amplified from MG1655 *E. coli* genomic DNA using the primers P10/P11. After digestion by NdeI and XhoI, PCR products were ligated into pET24a digested with the same enzymes, resulting in pET24-periLolE. The periLolE Hook was removed in a similar manner to that described for periLolC using two stages of PCR P10/P12 and P11/P13 and then an amplification of a mixture of the products with P10/P11. The resultant fragment was digested and ligated into pET24. The resultant plasmid, pET24-periLolE(ΔHook) encodes periLolE with residues 171-182 inclusive replaced by a Gly-Ala linker. Point mutations of LolA or periLolC were created by Quikchange site-directed mutagenesis from pET28-LolA or pET24-periLolC respectively using the primers listed in **Table S4**.

To target the periplasmic domain of LolC (wild-type or variant) to the periplasm, the region corresponding to residues 48-266 was amplified with primers P8/P14, digested BspHI-NotI and cloned into NcoI-NotI digested pET26b (Novagen). The entire region comprising periLolC with an N-terminal pelB secretion signal and C-terminal His-tag was then amplified with primers P15/P16, digested Xba-HindIII and introduced into pBAD18 (59) resulting in plasmid pBAD18-pelBperiLolC or indicated variant.

To express *E. coli* LolCDE with a His-tag on the C-terminus of LolD, the *lolCD* contiguous region was amplified with primers P17/P18 digested with PciI and NotI, and cloned into the first MCS (Multiple

Cloning Site) of pETDuet digested with the same enzymes. *lolE* was amplified with primers P19 and P20, digested NdeI-AvrII and introduced into the second MCS of the resulting plasmid to create pETDuet-LolCDE. Variants in LolCDE were created by a two-step PCR using mutagenic internal primers and P17/P18 or P19/P20 with pETDuet-LolCDE as template. After restriction enzyme digest, the variant *lolCD* or *lolE* PCR products were ligated into pETDuet-LolCDE from which the wild-type copies of *lolCD* or *lolE* had been excised. All clones were verified by DNA sequencing (Source BioScience).

Protein purification

Purification of wild-type and variant E. coli LolCDE

E. coli C43 (DE3) (58) carrying pETDuet-LolCDE or variants: LolC(R163A)DE, LolC(M175R)DE, LolC(E171Q)DE, LolC(ΔHook)DE, LolCDE(ΔHook) were grown in 2YT media supplemented with 100 μg/mL carbenicillin for 16h at 30 °C. Cells were pelleted at 3500 *g* for 15 min, resuspended in fresh media and protein expression induced with 1 mM IPTG. After 2.5 hours of induction at 30 °C, cells were harvested by centrifugation at 6000 *g* for 6 min and pellets frozen at -80 °C. Bacterial pellets were thawed at room temperature and resuspended in buffer composed of 50 mM Tris pH 7.5, 150 mM NaCl and 10 % (v/v) glycerol. Cells were then lysed by passage through a Constant Systems cell disruptor at 30200 psi. Unbroken cells and debris were removed by centrifugation at 10000 *g* for 10 min. Membranes were recovered from the supernatant by centrifugation at 115000 *g* at 5 °C for 2h and resuspended in the same buffer containing 1 % (w/v) DDM (dodecyl maltopyranoside) for solubilisation. After 1h, the soluble fraction was recovered by centrifugation (1h at 115000 *g*, 5 °C), supplemented with 40 mM imidazole and loaded on IMAC resin (Biorad Profinity) for 1h. The resin was washed with 50 mM Tris pH 7.5, 150 mM NaCl, 10 % (v/v) glycerol, 0.03 % DDM and 40 mM imidazole and the protein eluted with the same buffer containing 500 mM imidazole. Eluted LolCDE complex was buffer exchanged into 20 mM HEPES pH 7.5, 150 mM NaCl, 0.03 % DDM using either PD10 columns (GE Healthcare) or Amicon Ultra 100 kDa cut-off centrifugal concentrators and concentrated using the same device to 5-10 mg/mL before flash freezing and storage at -80 °C.

Purification of wild-type and variant E. coli LolC periplasmic domain

E. coli BL21 (DE3) cells bearing plasmid pET24-periLolC or pET24-periLolC(XnY) variant were grown in 1L of 2YT medium supplemented with 50 μg/mL kanamycin at 30 ºC. When the culture achieved an OD_{600} of 0.8 the temperature was reduced to 18 ºC and protein expression induced with 0.1 mM IPTG. After 16h further growth, cells were harvested by centrifugation at 4000 *g* and the pellet resuspended in 50 mL of 50 mM HEPES pH 7.5, 300 mM NaCl, supplemented with protease inhibitor cocktail (Roche), lysozyme and DNase. Bacteria were lysed by cell disruption (Constant Systems) at

30200 psi before removal of bacterial debris by ultracentrifugation (1h, 115000 *g* at 5 ºC). The soluble fraction was supplemented with 20 mM imidazole and loaded on to a 5 mL HisTrap FF column using an ÄKTAxpress FPLC (GE Healthcare). Bound proteins were washed with 15 column volumes (CV) of the same buffer, before elution with 250 mM imidazole. Peak fractions were analysed on SDS-PAGE and pooled according to purity in a 10 kDa exclusion size centricon filter (Amicon). Proteins were buffer exchanged into 20 mM HEPES pH 7.5, 150 mM NaCl using a 10 kDa cut-off centricon device (Amicon) and concentrated to 20-30 mg/mL, before flash freezing and storage at -80 °C. When required the C-terminal His-tag was removed using the Thrombin CleanCleave Kit (Sigma) according to the manufacturer's instructions.

Purification of E. coli wild-type and variant LolE periplasmic domain

The periplasmic domain of LolE and equivalent ΔHook variant were produced and purified as described for LolC with a purification buffer composed of 50 mM Tris pH 8.0, 300 mM NaCl and 10 % (v/v) glycerol and a desalting buffer comprising 20 mM HEPES pH 7.5, 150 mM NaCl and 5 % (v/v) glycerol. Proteins were stored at -80 °C at 15 mg/mL.

Purification of E. coli wild-type LolA and LolA F47E

Wild-type and LolA F47E proteins were produced in *E. coli* BL21 (DE3) bearing pET28-LolA or pET28-LolA(F47E). Cells were grown at 37 °C in 1L of 2YT medium supplemented with 50 µg/mL kanamycin. Cultures were induced with 0.1 mM IPTG when an OD_{600} of 0.8 was reached and temperature was reduced to 18 °C. After 16h, bacteria were harvested by centrifugation at 4000 *g* and resuspended in a buffer composed of 50 mM Tris, pH 8.0, 300 mM NaCl before lysis in a cell disruptor (Constant Systems) at 30200 psi in the presence of lysozyme and DNase. Cell debris were removed by ultracentrifugation (1h, 115000 *g* at 5 ºC). The soluble fraction was supplemented with 20 mM imidazole and loaded onto a 5 mL HisTrap FF column using an ÄKTAxpress system (GE Healthcare). Bound proteins were washed with 15 CV of the same buffer, before elution with 250 mM imidazole. Peak fractions were analysed on SDS-PAGE and pooled in a 10 kDa cut-off centrifugal concentrator (Amicon). Proteins were then buffer exchanged into 20 mM HEPES at pH 8.0 and 200 mM NaCl and concentrated to 25 mg/mL. When required, the N-terminal His-tag was removed using the Thrombin CleanCleave Kit (Sigma) according to the manufacturer's instructions. After cleavage, the protein was re-purified using Ni-IMAC to remove free His-tags and uncleaved His-tagged protein.

Purification of E. coli wild-type soluble LolB

Soluble LolB was produced in *E. coli* BL21 transformed with pET28-mLolB and purified as described for wild-type LolA with a buffer composed of 20 mM Tris pH 7.4, 150 mM NaCl and 0.25 mM TCEP. The protein was desalted with the same buffer containing no TCEP. Proteins were stored at -80 °C at 30 mg/mL.

Size-exclusion chromatography analysis

Size-Exclusion Chromatography (SEC) was performed on a Superdex 75, 10/300 GL column run at 0.8 mL/min using an ÄKTA Pure FPLC system (GE Healthcare) equipped with a 100 µL injection loop. The running buffer was composed of 20 mM HEPES at pH 7.5, 150 mM NaCl. For analysis of individual proteins, 0.5 mg of protein was loaded onto the column. To assess the interaction of two proteins, 0.5 mg of each protein was mixed and incubated for 5 minutes prior to injection.

Isothermal titration calorimetry (ITC)

ITC experiments were carried out at 25 °C in a VP-ITC calorimeter (MicroCal, GE Healthcare) by injecting 300 or 450 µM of wild-type or variant LolC periplasmic domain into 25 µM LolA. ITC buffer was composed of 20 mM HEPES pH 7.5, 200 mM NaCl. Initially 5 µL was injected over 10 s followed by injections of 10 µL over 20 s until the syringe was empty. Injections occurred every 200 s and the cell stirring speed was 300 rpm. To characterise the interaction of LolA and LolE, LolA (450 µM) was injected into the cell containing 25 µM periplasmic LolE while LolA F47E (200 µM) was injected into 25 µM LolC periplasmic domain. For each titration, a control run with injectant and buffer alone in the cell was performed. The resulting signal was subtracted as a linear fit from protein-protein data. Binding affinity, stoichiometry and thermodynamic parameters were obtained by nonlinear least-squares fitting of experimental data using a single-site binding model from the Origin software package.

Crystallization and structure determination

All crystals were grown at 15 °C by the sitting drop vapour diffusion method over a reservoir of 80 µL in MRC 2-drop plates (Molecular Dimensions).

LolA·LolC complex

Individually purified LolC periplasmic domain and LolA were incubated together (both at a final concentration of 6 mg/mL) in 20 mM HEPES pH 7.5, 150 mM NaCl and then mixed with the precipitation solution at a 1:1 ratio in a final volume of 1 µL over a reservoir of 80 µL. Crystals of the LolA·LolC complex were obtained in 100 mM HEPES pH 6.5, 45 % (w/v) poly(acrylic acid sodium salt) 2100. Crystals were obtained after two days following seeding with crushed crystals of LolA F47E and LolC periplasmic domain obtained in 13-17 % PEG 8000, 10-20 % (v/v) glycerol and 30-60 mM KH_2PO_4. The cryoprotective solution was composed of the reservoir solution supplemented with 20 % ethylene glycol. Data were collected on beamline ID30B at ESRF. The structure was solved by molecular refinement with Phaser (53) using the wild-type LolC periplasmic domain (5NAA) after trimming residues 48-63, 170-179, 252-273 and LolA (1IWL) after removing loops corresponding to amino acids 115-124 and 180-182. Iterative cycles of density modification with Parrot (60) and automated model building with Buccaneer (61) produced a model that was further improved with several

rounds of Refmac (55) and manual building in Coot (54). Extra density present at the interface of LolA monomers was consistent with indole (**Figure S9**). Indole was positively identified in the growing bacterial culture using Kovac's reagent but not in the protein solution, possibly due to insensitivity of the test. Consequently, indole was not included in the final coordinate file (PDB 6F3Z).

LolA F47E mutant

Crystals of LolA F47E protein were obtained by mixing 0.5 µL of protein at 12 mg/mL in 20 mM HEPES pH 7.5, 150 mM NaCl with the same volume of a precipitant solution composed of 13 % (w/v) PEG 8000, 20 % (v/v) glycerol. No seeding procedure was used. Crystals appeared after three days and were cryoprotected in the reservoir solution containing glycerol at a final concentration of 36 % (v/v) before being frozen in liquid nitrogen. X-ray diffraction data were obtained at Diamond (UK) on beamline I03 equipped with a Pilatus3 6M detector. LolA (1IWL) was used as a search model in Phaser (53) for molecular replacement after trimming residues 1-26, 32-51 and 88-161. After a round of refinement in Refmac (55), a new set of phases was generated by density modification using Parrot (60). The final model was obtained after a round of auto-building with Buccaneer (61), manual manipulation using Coot (54) and refinement with Refmac (55).

LolC ΔHook periplasmic domain

LolC periplasmic domain lacking the Hook (Δ167-179 GA) was crystallised similarly to LolA F47E with protein concentrated to 12 mg/mL and a precipitant solution composed of 30 % (w/v) PEG 2000 MME, 150 mM sodium acetate pH 4.6, 200 mM ammonium sulfate. Seeds of wild-type LolC periplasmic domain were used to favour crystallization. Crystals were flash-frozen in liquid nitrogen after a brief immersion in the precipitation solution supplemented with 20 % (v/v) glycerol as cryoprotectant. Data were collected under cryogenic conditions on beamline ID30B at ESRF (Grenoble, France) on a Pilatus3 6M detector. Images were integrated with Imosflm (51) and scaled with Aimless from the CCP4 suite (52). Structure was refined by molecular replacement with Phaser (53) using the wild-type LolC periplasmic domain structure (5NAA) as the molecular replacement probe. The atomic model was manually built in Coot (54) and refined with Refmac (55) using NCS restraints.

Structure depositions

Structures were deposited in the Protein DataBank with accession codes **6F3Z** (LolA·LolC complex), **6F49** (LolC ΔHook), and **6FHM** (LolA F47E variant).

Measurement of LolCDE ATPase activity

The ATPase activity of LolCDE proteins was evaluated using the EnzCheck Phosphate Assay Kit (Thermofisher) that couples the release of inorganic phosphate to purine nucleoside phosphorylase (PNP) mediated breakdown of 2-amino-6-mercapto-7-methyl-purine riboside (MESG). One unit of PNP

enzyme was added to a reaction mix containing 50 mM Tris-HCl pH 7.5, 1 mM $MgCl_2$, 0.1 mM azide, 500 μM MgATP (saturating concentration), 200 μM MESG and 0.03 % DDM in a final volume of 350 μL. The mixture was incubated for 3 minutes and the reaction initiated with addition of 1 μM LolCDE (wild-type or variant). The reaction was followed spectrophotometrically at 360 nm using a NanoPhotometer (Implen). Where indicated, the LolCDE inhibitor, Compound 2 (20), was added at 10 or 100 μM in 1 % DMSO (final concentration) and compared to addition of 1 % DMSO alone. To assess the effect of LolA on LolCDE ATPase activity, 5 μM untagged LolA (a five-fold molar excess) was incubated with LolCDE for 3 minutes prior to initiation of the reaction. The rate of hydrolysis was calculated using GraFit 7.0.3 software from the slope of the initial linear phase of the reaction. A calibration curve obtained using known concentrations of phosphate was used to convert absorbance readings to meaningful units.

Periplasmic targeting of LolC domain

Overnight cultures of C43 (DE3) cells bearing plasmid pBAD18-pelBperiLolC or indicated variant were grown overnight at 37 ºC in LB supplemented with 0.5 % (v/v) glycerol and 100 μg/ml carbenicillin. Cultures were diluted to an OD_{600} of 0.02 in fresh medium and grown at 37ºC. After 45 minutes, 0.2 % (w/v) arabinose (final concentration) was added to induce protein expression and the growth followed by monitoring OD_{600} for a further 4 hours. To assess expression of the LolC constructs in the periplasm, cultures were inoculated as described above and centrifuged at 3000 *g* for 30 minutes at 4 ºC after 60 minutes growth post-induction. Cells resuspended in 200 mM Tris, 500 mM sucrose, 1 mM EDTA, incubated on ice for 30 mins. Following centrifugation at 16000 *g* for 30 minutes at 4 ºC, the supernatant was taken as the extracytoplasmic fraction. Samples were resolved on SDS-PAGE, transferred to nitrocellulose membrane, and immunoblotted with anti-His (Qiagen) and a dye-conjugated Donkey anti-mouse secondary (Licor) antibodies. Immunoblots were revealed using an Odyssey Licor fluorescence imager.

IMAC-based LolA binding assay

His-tagged LolC periplasmic domain (15 μM final concentration) in 20 mM Hepes pH 7.5, 150 mM NaCl, in a final volume of 250 μL was incubated with 100 μL of Ni-IMAC resin (Biorad) for 5 minutes in a microbatch spin column (Generon). Non-tagged LolA (15 μM final concentration) was then added. After a further 5 minutes, the resin was washed three times with 250 μL of buffer before elution of bound proteins with the same volume of buffer containing 250 mM imidazole. Eluted proteins were analysed on gradient SDS-PAGE gels with purified proteins as references. Interaction of His-tagged LolCDE with LolA was assessed in the same manner except that 0.01 % DDM was added to all buffers. To assess the effect of any endogenously bound nucleotide, LolCDE was incubated with 5 mM EDTA, the sample desalted and the experiment performed as described above. Where specified, 1 mM MgATPγS or MgATP (final concentration) were added during incubation, wash and elution steps.

Where indicated, 25 or 100 μM of Compound 2 inhibitor (21), dissolved in 1 % DMSO (final concentration), was incubated with the His-tagged protein prior to addition of LolA and the effect compared to addition of DMSO alone. To assess interaction between LolB and the LolC periplasmic domain, the binding assay was performed with His-tagged mature LolB and untagged LolC and compared to the interaction of His-tagged LolA with untagged LolC.

Construction of LolCDE homology model

The LolCDE homology model was built with assistance from the PHYRE2 server (62). LolD and the inner membrane helices of LolC and LolE were built using the MacB structures 5LIL and 5NIL as respective models for the closed and open state. The periplasmic domain of LolC comes from the LolA·LolC structure (6F3Z) in which LolC Sabre and Porter subdomains were split and separately aligned to corresponding Sabre and Porter domains of MacB in the open (5NIL) or closed state (5LIL). LolA was positioned according to the coordinates of the LolA·LolC structure (6F3Z) which was superposed onto the homology model Sabre subdomain. The periplasmic domain of LolE was built with PHYRE2 using the structure of LolC periplasmic domain (5NAA) as a template. The Sabre and Porter subdomains of LolE were separated and placed in the same manner described for those of LolC.

Sequence alignments

The multiple and structure alignment server PromalS3D (63) was used to align the amino acid sequences of LolC, LolE, LolF, MacB and PvdT. The nucleotide binding domain of MacB and PvdT proteins were excluded from the alignment.